universität wien

MASTERARBEIT / MASTER'S THESIS

Titel der Masterarbeit / Title of the Master's Thesis

„Computational dielectric spectra of amino acids in electrolyte solutions“

verfasst von / submitted by

Marion Sappl, BSc BA

angestrebter akademischer Grad / in partial fulfilment of the requirements for the degree of

Master of Science (MSc)

Wien, 2023 / Vienna, 2023

Studienkennzahl lt. Studienblatt / degree programme code as it appears on the student record sheet:	UA 066 862
Studienrichtung lt. Studienblatt / degree programme as it appears on the student record sheet:	Masterstudium Chemie
Betreut von / Supervisor:	Univ.-Prof. Dipl.-Chem. Dr. Christian Schröder

Acknowledgements

First and foremost I want to thank my supervisor Univ.-Prof. Dipl.-Chem. Dr. Christian Schröder for making this thesis possible and incorporating me into this team so sincerely. I want to thank Florian Jörg and András Szabadi for supporting me during my research and helping me with difficulties I encountered. Furthermore, I want to thank Márta Gődény and Johannes Karwounopoulos for making my stay not only educational but also delightful. Special thanks goes out to Christian Fellinger for his previous work on the project.

I want to thank my parents, Gabriele and Robert Sappl for supporting me during my studies and generating enthusiasm for diving into uncharted learning territories during my childhood. I want to thank my sister, Lisa Sappl whom I've always had the most interesting talks about science with and who could provide the insight to questions about physics.

Abstract

Specific ion effects have been known for over 200 years. However, the exact impact of various ions are still not predictable in a reliable manner. This Master's Thesis explores the effects of different salts on the dielectric spectra of amino acids to gain insight on the interactions between amino acids and salts. The investigated amino acids are arginine, lysine and serine in electrolyte solutions with potassium bromide, chloride and iodide as well as lithium and sodium chloride. The amino acids were tested in solutions with varying concentrations using molecular dynamics simulations. The simulations were evaluated and the results were compared to experimental data to validate the output. The dielectric spectra were evaluated regarding the permittivity and relaxation times of the respective components. Here, specific ion effects were observable often in accordance to the Hofmeister series. To investigate the root of the specific ion effects structural analyses were carried out. Radial distribution functions and radial dipole-dipole spatial correlation functions were used to characterize the structural alignment of the molecules and their dipole moments.

Kurzfassung

Ionenspezifische Effekte sind seit über 200 Jahren bekannt. Trotzdem sind die genauen Auswirkungen verschiedener Ionen auf Aminosäuren immer noch nicht zuverlässig vorhersehbar. Diese Masterarbeit beschäftigt sich mit den Auswirkungen verschiedener Salze auf dielektrische Spektren von Aminosäuren um einen tieferen Einblick in die Wechselwirkungen zwischen Aminosäuren und Salzen zu bekommen. Die untersuchten Aminosäuren sind Arginin, Lysin und Serin im Zusammenspiel der Salze Kaliumbromid, -chlorid und -iodid sowie Lithium- und Natriumchlorid. Die Aminosäuren wurden in Elektrolytlösungen der jeweiligen Salze mit unterschiedlichen Salzkonzentrationen mittels molekulardynamischer Simulationen analysiert. Die Simulationen wurden ausgewertet und die Ergebnisse mit experimentellen Daten zur Überprüfung verglichen. Die dielektrischen Spektren wurden bezüglich der Permittivität und Relaxationszeiten der Komponenten ausgewertet. Hierbei konnten ionenspezifische Effekte ausgemacht werden. Es stellt sich heraus, dass das Ausmaß der Auswirkungen in vielen Fällen analog zur Hofmeister Serie sind. Um die Ursache der Ionenspezifischen Effekte zu untersuchen wurden strukturelle Analysen, die die räumliche Anordnung der Moleküle und deren Dipolmomente charakterisiert, durchgeführt. Dafür wurden radiale Verteilungsfunktionen und räumliche Dipol-Dipol Korrelationsfunktionen untersucht.

Contents

1 Introduction

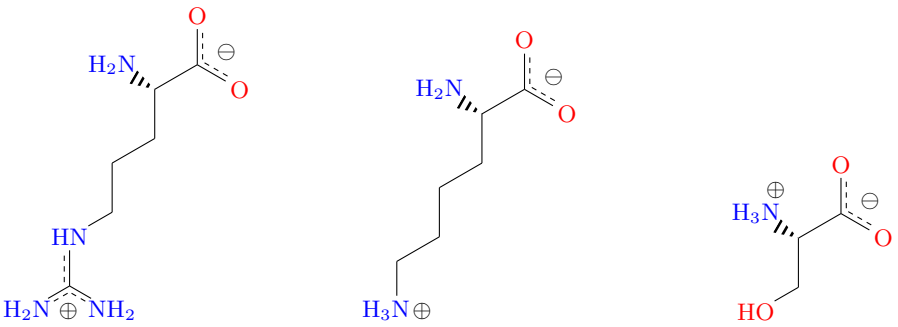

(a) L-Arginine (b) L-Lysine (c) L-Serine

Figure 1.1: Structures of the zwitterionic amino acids under investigation.

The principle of the Hofmeister series is that ions and molecules have varying effects on the structure and stability of proteins and other macromolecules in solution. The Hofmeister series describes salts in their relation to chaotropic and kosmotropic effects. Chaotropic ions usually reduce the stability but increase the solubilization. Kosmotropic ions do the opposite. Franz Hofmeister described salt specific effects precipitating egg white proteins based on Lewith's previous work on blood serum globulin [1]. The Hofmeister series helps to understand how different ions affect the behavior of biomolecules in solution. The specific ion effects on which the Hofmeister series is based on however, are observable in many other properties throughout different fields as medicine, biology, chemistry and industrial science [2]. Even though the Hofmeister series has been discovered over 100 years ago there is still no reliable prediction possible on the specific ion effects and its magnitude [2]. Previous studies have focused on the ion specific effects on proteins and their interactions [3–5]. The Hofmeister series has not been an intensely studied subject in relation to zwitterionic amino acids in solution.

As amino acids and water are dielectric active substances, solutions of amino acids can be characterized by dielectric spectroscopy. The ability of electrolytes changing the dielectric behavior of water has been studied thoroughly [6–12]. There have also been studies on dielectric spectroscopy of aqueous amino acid solutions [13–18]. However, the specific ion effects on dielectric spectra of amino acids in aqueous solutions haven't gained much attention. This Master's Thesis studies ion specific effects of different salts from the Hofmeister series on different amino acids. Non polarizable molecular dynamics simulations will be used to calculate the dielectric spectra of different amino acids and salts. The results of this thesis are compared to dielectric spectroscopic measurements from collaborators of the Max Planck Institute for Polymer Research in Mainz.

1.1 Systems under investigation

The amino acids investigated in this Master's Thesis are L-arginine, L-lysine and L-serine as zwitterions, visualized in figure 1.1. These three amino acids were chosen as they showed the strongest specific ion effects in the dielectric spectra during experiments. To study cationic effects chlorides of lithium, sodium and potassium were chosen. To study anionic effects potassium chloride, bromide and iodide were investigated. The amino acids were all examined in aqueous solutions with salt concentrations up to twice the molar amino acid concentration. The concentration of the amino acids and salts were chosen so that there was no precipitation.

2 Theory

2.1 Hofmeister Series and specific ion effects

The Hofmeister Series, named after Franz Hofmeister, who thoroughly described salts according to their ability to precipitate proteins [1], categorizes ions according to their specific ion effects [2]. The ions are often categorized as kosmotropic and chaotropic ions, describing whether or not hydrogen bonding in water molecules are promoted and diminished, respectively [19, 20]. The Hofmeister Series is used to predict a vast variety of ion specific effects such as surface tension, solubility, interfacial potential, colloidal stability, and biological activity [21]. In this Master's Thesis the chlorides of lithium, sodium and potassium were investigated to study cationic effects. Anionic effects were evaluated on potassium chloride bromide and iodide. The ions ordered according to their kosmotropic and chaotropic behavior are depicted in figure 2.1.

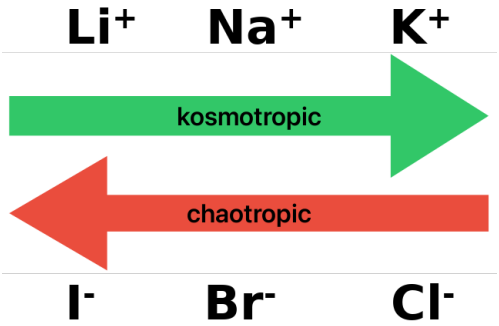

Figure 2.1: Cations and anions investigated in this thesis in their relative order according to the Hofmeister series.

After the study conducted by Hofmeister, specific ion effects were investigated extensively. Specific ion effects refer to the phenomenon where the behavior of a system, particularly in the context of solutions or colloidal suspensions, is influenced by the specific types and concentrations of ions present. These effects can manifest in a variety of ways, including alterations in solubility, chemical reactivity, aggregation, and stability of colloids or macromolecules. There have been many theories to why specific ion effects manifest in they way they do, however there are multiple factors at play. One important factor is the solvation of the ions in the solvent, mostly water. It used to be believed, that the long range structure of water is the reason for ion specific behavior [22]. However, the structure of water seems to be mostly affected in the first solvation shell [22, 23]. Until today no reliable predictive theory has been able to explain ion specificity [2]. This is due

to the complex nature of interactions of ions with hydrophilic and hydrophobic groups, co-solutes and interfaces [2].

2.2 Molecular dynamics simulations

In this introduction to molecular dynamic (MD) simulations, we will delve deeper into the theoretical foundation, key components of force fields, simulation techniques, and applications that make this approach an indispensable tool for modern-day molecular research. Additionally, we will explore its limitations and the challenges faced when modeling large, complex molecular systems. Ultimately, molecular mechanics serves as a bridge between theoretical concepts and experimental observations, providing valuable insights into the intricate world of molecules and their interactions.

2.2.1 Molecular mechanics

Molecular mechanics is a computational method used in the field of theoretical chemistry and molecular biology to study the behavior of molecules and their interactions. It is a fundamental approach that simulates the motion and energy of molecular systems, enabling researchers to gain valuable insights into the structure, dynamics, and properties of various chemical and biological systems at the atomic level. The underlying principle of molecular mechanics is rooted in classical mechanics, which describes the motion of particles based on Newton's laws of motion.

$$\vec{p}_i = m_i \cdot \vec{\nu}_i \tag{2.1}$$

Newton's second law of motion states that the time derivative of the momentum is the force:

$$\vec{F}_i = \frac{d\vec{p}_i}{dt} \tag{2.2}$$

With constant masses one gets:

$$\vec{F}_i = m_i \cdot \vec{a}_i \tag{2.3}$$

In the context of molecular systems, the atoms within a molecule are represented as individual particles, and their interactions are approximated using empirical force fields. These force fields consist of a set of mathematical equations and parameters that define the potential energy surfaces and forces between atoms.

The force acting on a particle can also be described as the negative gradient of the potential energy of that particle:

$$\vec{F}_i = -\frac{\partial U}{\partial r_i} = -\left(\frac{\partial U}{\partial x_i}, \frac{\partial U}{\partial y_i}, \frac{\partial U}{\partial z_i}\right) \tag{2.4}$$

2.2.2 Force fields

In MD simulations, force fields are models used to describe the potential energy acting on atoms within a molecular system. They are at the core of the simulation, dictating how the atoms interact with each other and how the system evolves over time.

Different force fields, such as CHARMM, AMBER, and GROMOS, have been developed over the years, each with its strengths and limitations. Researchers choose the appropriate force field based on the specific molecular system and properties they aim to investigate. While force fields provide valuable insights into molecular behavior, it is essential to recognize that they are simplified representations of complex quantum mechanical interactions, and they have inherent limitations, especially for extremely large or highly charged systems.

The interactions can be parted into bonded U_{bonded} and non bonded $U_{nonbonded}$ interactions.

$$U_{total} = U_{bonded} + U_{nonbonded} \tag{2.5}$$

Bonded Interactions

Bonded interactions consist of bond, angle, dihedral angle and improper angle potentials:

$$U_{bonded} = U_{bond} + U_{angle} + U_{dihedral} + U_{improper} \tag{2.6}$$

U_{bond} describes the covalent bonds between atoms within a molecule. The potential to describe bonds in molecular physics is usually the Morse potential. The force fields used in MD simulations use harmonic potential energy functions to represent bond stretching, which is based on Hooke's law to save computing time. A comparison of Morse potential and harmonic potential is shown in figure 2.2. The force constant and equilibrium bond length determine the strength and length of the bond, respectively. Usually in MD simulations the current distance is so close to the equilibrium value, that the harmonic and Morse potential do not differ much. In classic MD simulations bonds cannot be broken or formed.

$$U_{bond} = \sum_{bonds} k_b(r - r_{eq})^2 \tag{2.7}$$

Where k_b is the force constant, r is the bond length and r_{eq} is the equilibrium bond length.

U_{angle} describes the angular potentials between connected atoms. Similarly to the bond interactions, force fields typically use harmonic potentials to represent angle bending, with the force constant k_θ and equilibrium angle θ_{eq} defining the angular potential.

$$U_{angle} = \sum_{angles} k_\theta(\theta - \theta_{eq})^2 \tag{2.8}$$

Torsional or dihedral interactions are described by $U_{dihedral}$. Torsional interactions account for the rotation around single bonds. The potential energy for dihedral angles is

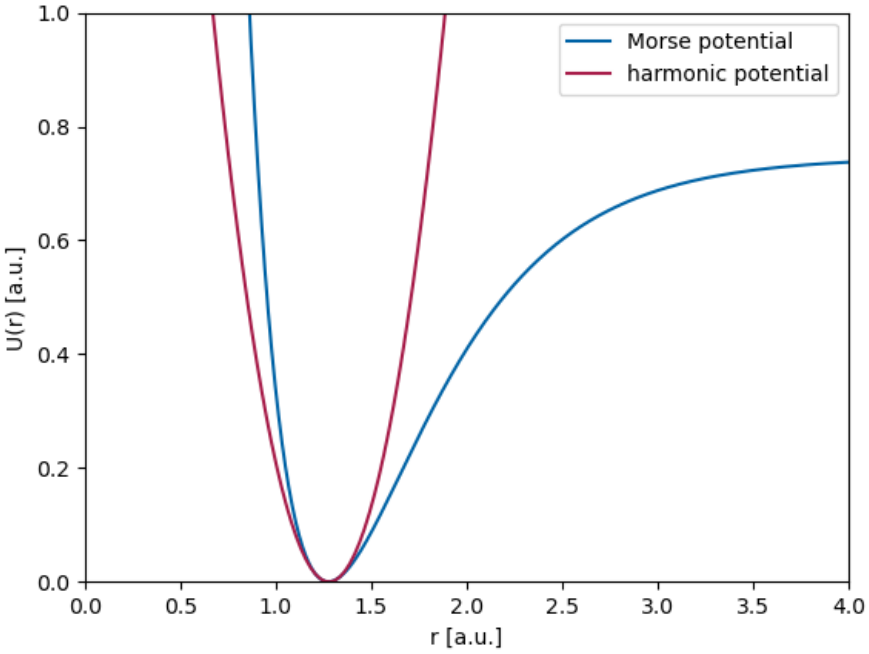

Figure 2.2: Comparison of Morse and harmonic potential.

typically described using a periodic function with multiple terms, each corresponding to a specific conformation of the molecule. These terms represent the energy barrier k_ϕ and periodicity n of the torsion angle ϕ.

$$U_{dihedral} = \sum_{dihedrals} k_\phi[1 + cos(n\phi + \delta)] \tag{2.9}$$

The improper angle ω is the angle between the atom in question and an imaginary plane formed by three other atoms. $U_{improper}$ describes these interactions, usually analogous to bond and angle interactions as an harmonic oscillator:

$$U_{improper} = \sum_{impropers} k_\omega(\omega - \omega_{eq})^2 \tag{2.10}$$

Non-bonded interactions

Non-bonded interactions are the forces governing the interactions between atoms that are not connected. There are two types of non-bonded interactions, electrostatic and van der Waals (vdW) interactions:

$$U_{non-bonded} = U_{vdW} + U_{electrostatic} \tag{2.11}$$

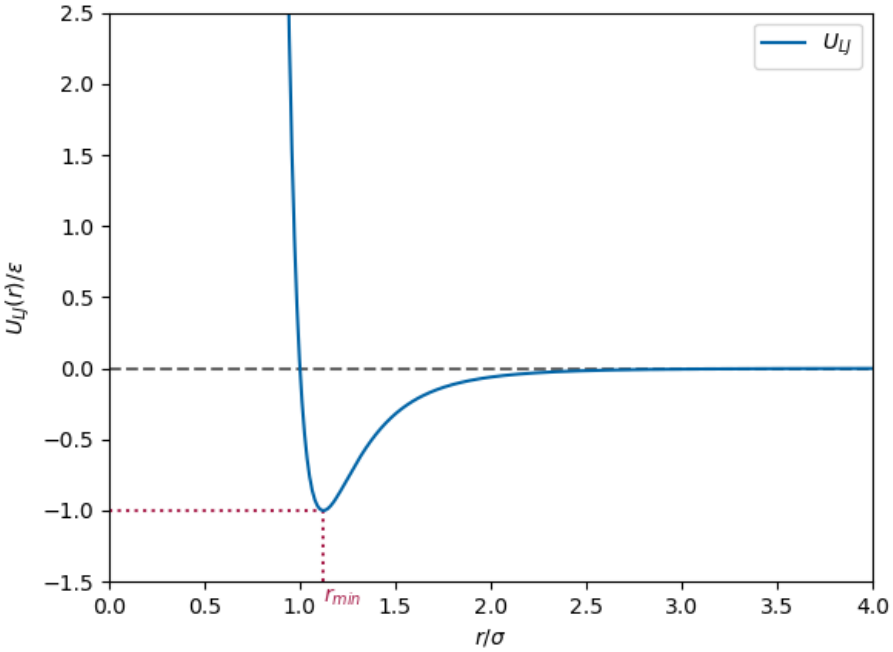

Figure 2.3: Lennard-Jones potential. The radius at potential minimum r_{min} is at $\sqrt[6]{2}\sigma$.

Van der Waals interactions are typically represented by the Lennard-Jones potential [24]. The Lennard-Jones potential is visualized in figure 2.3.

$$U_{vdW} = U_{LJ} = \sum_i \sum_{j>i} 4\epsilon_{ij} \left\{ \left(\frac{\sigma_{ij}}{r_{ij}} \right)^{12} - \left(\frac{\sigma_{ij}}{r_{ij}} \right)^{6} \right\} \tag{2.12}$$

Where σ_{ij} is the collision diameter and ϵ_{ij} is the potential well depth [24]. The potential considering both attractive van der Waals forces that varies as r^{-6} and a repulsive part that varies with r^{-12} [24].

To obtain interactions between different atom types the Lorentz-Berthelot mixing rules are applied [24]. The Lorentz rule calculates the arithmetic mean from the values of the pure species and is used for σ_{ij} [24]:

$$\sigma_{ij} = \frac{\sigma_{ii} + \sigma_{jj}}{2} \tag{2.13}$$

ϵ_{ij} is calculated using the Berthelot rule taking the geometric mean of the values for the pure species [24]:

$$\epsilon_{ij} = \sqrt{\epsilon_{ii}\epsilon_{jj}} \tag{2.14}$$

Electrostatic interactions arise due to the charges of atoms. Force fields typically use Coulomb's law to calculate the energy and forces, considering the partial charges on the atoms.

$$U_{electrostatic} = U_{Coulomb} = \sum_{i} \sum_{j>i} \frac{q_i q_j}{4\pi\varepsilon_0 r_{ij}} \tag{2.15}$$

2.3 Dielectric spectroscopy

Dielectric spectroscopy is a technique used to study the electrical properties of materials as a function of frequency. It provides insights into the behavior of materials in response to electric fields, giving information on their molecular and structural properties, as well as their interactions with electromagnetic radiation.

Dielectric spectroscopy involves the application of an alternating electric field to a material and the measurement of its electrical response over a range of frequencies [25]. The dielectric properties of a material are characterized by its permittivity (ε) and conductivity (σ) [26]. These properties depend on the material's composition, temperature, and the frequency of the applied electric field [27].

The dielectric permittivity (ε) quantifies how a material responds to an electric field. It represents the ability of a material to store electrical energy when subjected to an electric field. Materials with high dielectric constants are good insulators, while those with low dielectric constants are poor insulators.

The permittivity is in general a complex quantity, consisting of a real part (ε') and an imaginary part (ε''):

$$\varepsilon^*(\omega) = \varepsilon'(\omega) - i\varepsilon''(\omega) \tag{2.16}$$

Where $\varepsilon^*(\omega)$ is the complex dielectric permittivity, $\varepsilon'(\omega)$ is proportional to the energy stored reversibly in the system per period and $\varepsilon''(\omega)$ is proportional to the energy dissipated per period [28].

Dielectric spectroscopy measures the dielectric properties of a material across a wide range of frequencies, typically from millihertz to gigahertz or even higher [25]. Different frequency ranges reveal different information about the material's behavior.

Dielectric spectroscopy finds applications in various fields, including:

- Material Characterization: It helps determine the structure, and composition of materials [29].
- Biological Studies: In biology, it is used to study the dielectric properties of cells, tissues, and biomolecules, aiding in areas such as cell viability assessment and cancer diagnosis [30, 31].
- Polymers and Nanomaterials: It is valuable for studying the electrical properties of polymers, nanomaterials, and composites, aiding in the development of advanced materials [25, 32].

- Food Science: It is used to assess the quality and freshness of food products [33, 34].
- Electronics: Dielectric spectroscopy is crucial for the design and evaluation of electronic components, such as electrodes [35].

In computational chemistry the complex permittivity can be calculated from the collective dipole moment. The collective dipole moment can be expressed as [26]:

$$M_{tot}(t) = \sum_i \sum_\alpha q_{i,\alpha} \cdot r_{i,\alpha}(t) \tag{2.17}$$

Where $M_{tot}(t)$ is the time dependent collective dipole moment, $q_{i,\alpha}$ and $r_{i,\alpha}$ are the charge and position of the atom α of molecule i.

The collective dipole moment can be decomposed into a translational M_J

$$M_J(t) = \sum_i \sum_\alpha q_{i,\alpha} \cdot r_{com,i}(t) = \sum_i q_i \cdot r_{com,i}(t) \tag{2.18}$$

and a rotational part M_D

$$M_D(t) = M_{tot}(t) - M_J(t) = \sum_i \sum_\alpha q_{i,\alpha} \cdot (r_{i,\alpha}(t) - r_{com,i}(t)) \tag{2.19}$$

with $r_{com,i}(t)$ being the position of the center of mass of the molecule i and q_i being its charge [26]. Considering this, only charged species contribute to M_J. M_D is the sum of all non-translational motions, e.g. all rotations and molecular vibrations. M_D is referred to as the collective rotational dipole moment since the rotation around the center of mass is the dominating process [26].

To calculate dielectric spectra one can use the time correlation function of the collective dipole moment [26]:

$$\Sigma_0(\omega) = \Sigma^*(\omega) - \big(\varepsilon_\infty - 1\big) = \frac{4\pi}{3Vk_BT}\mathcal{L}\left[-\frac{d}{dt}\langle M_{tot}(0) \cdot M_{tot}(t)\rangle_{eq}\right] \tag{2.20}$$

With $\Sigma_0(\omega)$ being the generalized dielectric constant, ε_∞ being the permittivity at $\omega = \infty$, V being the volume, k_B the Boltzmann constant, T the temperature, and $\mathcal{L}$ the Fourier-Laplace transform operator. In classical non-polarizable MD $\varepsilon_\infty = 1$.

The time correlation function of M_{tot} can be expressed as

$$\Phi_{tot} = \langle M_{tot}(0) \cdot M_{tot}(t)\rangle \tag{2.21}$$

and as

$$M_{tot} = M_D + M_J \tag{2.22}$$

it can be further decomposed to

$$\Phi_{tot} = \langle M_D(0) \cdot M_D(t)\rangle + 2\langle M_D(0) \cdot M_J(t)\rangle + \langle M_J(0) \cdot M_J(t)\rangle. \tag{2.23}$$

In this work, the only charged species are ions and are fully solvated. As the simulations were all chosen to be non polarizable, the ions themselves do not have a dipole moment. Therefore, the ions do not contribute to M_D. Furthermore, due to the solutions being diluted, the dielectric conductivity ($\vartheta(\omega)$) is small, leading to negligible values for the correlation functions $\langle M_D(0) \cdot M_J(t) \rangle$ and $\langle M_J(0) \cdot M_J(t) \rangle$. Therefore the dielectric spectra were calculated as:

$$\Sigma_0(\omega) = \varepsilon(\omega) = \frac{4\pi}{3Vk_BT} \mathcal{L}\left[-\frac{d}{dt}\langle M_D(0) \cdot M_D(t) \rangle_{eq}\right] \tag{2.24}$$

2.4 Radial distribution functions

The radial distribution functions (RDFs), also known as pair distribution functions, are mathematical functions to describe the spatial distribution of particles in a system, such as atoms, molecules, or ions. RDFs are useful for characterizing the local structure and arrangement of particles within a bulk material or a fluid.

The RDF quantifies how the density of particles varies with distance from a reference particle within the system. It provides information about the probability of finding another particle at a certain distance from the reference particle. In simple terms, it answers the question: "Given a particle at a specific location, what is the likelihood of finding another particle at a certain distance away?"

The RDF characterizes the relationship between one species' j local density surrounding a reference site ri and its mean density ρ [36]. It is typically defined as [36]:

$$g_{000}(r) = \frac{1}{\rho 4\pi r^2 dr} \sum_j \langle \delta(r - |r_{ij}|) \rangle \tag{2.25}$$

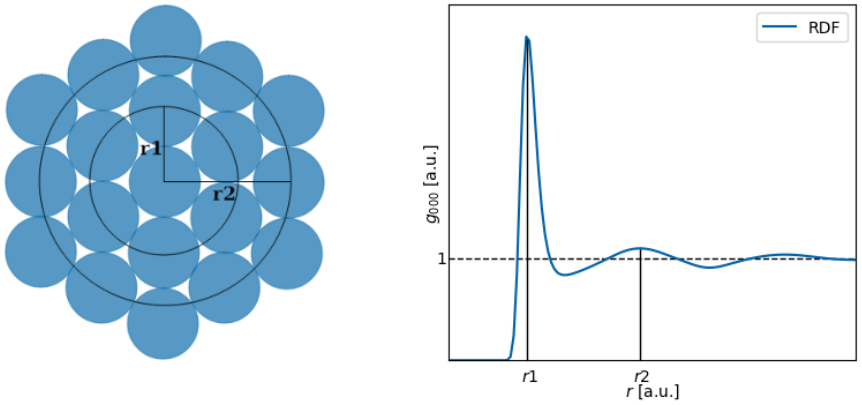

Figure 2.4: Visualisation of the g_{000} function. The radii r1 and r2 are where there is the highest density of particles from a central particle. At high radii the function becomes one, as the local density is approximately the global density.

Where $\delta(r - |r_{ij}|)$ is the Dirac delta function, which is 1 when $|r_{ij}|$ is approximately equal to r (the distance from the reference particle), and 0 otherwise. Visually the RDF can be imagined as the density of particles inside the shell of a spherical shell with a thickness of dr and a diameter of r compared to the average density. The species i and j are commonly defined as atoms, however they can also be defined with respect to the center of mass of a molecule. A visualization of the RDF is depicted in figure 2.4.

2.4.1 Dipole-dipole spatial correlation function

The orientation of dipolar species can give important information for interpreting dielectric spectra. To obtain information a special case of spatial correlation functions can be used, which is related to the RDF. The angular correlation function g_{110} weighs the RDF with the cosine of the angle between the dipole moments μ_i and μ_j [36].

$$g_{110}(r) = \frac{1}{\rho 4\pi r^2 dr} \sum_j \langle cos(\mu_i, \mu_j)\delta(r - |r_{ij}|)\rangle \tag{2.26}$$

If $0 \leq cos(\mu_i, \mu_j) < \pi/2$, the function is positive, meaning the dipoles point in the same direction. If $\pi/2 < cos(\mu_i, \mu_j) \leq \pi$, the function is negative with the dipoles pointing in opposite directions. At $cos(\mu_i, \mu_j) = \pi/2$ the dipoles are orthogonal. The directions of dipoles strongly affects the dielectric permittivity. For example acetic acid has a low permittivity even though it has a high dipole moment due to dimerization [37].

3 Methods

3.1 Simulation setup

The simulation boxes were packed with PACKMOL [38]. All simulations were carried out using OpenMM [39]. Equilibration was done in an NPT ensemble for 1 ns, production was done in an NVT ensemble with a total simulation time of 100 ns each. All molecular dynamic simulations were non-polarizable. In sum there were five replicas done for each system. The exact packing numbers for particles are listed in table 3.1 for arginine systems, table 3.2 for lysine systems and table 3.3 for serine systems. The packing numbers are the same for all tested water models and force fields.

3.1.1 Molecule parameterization

The topology of all cations and anions as well as SPCE water were taken from the CHARMM-GUI [40] website CHARMM [41] Small Molecule Library (CSML). The topology of the zwitterionic amino acids were generated using ACPYPE [42]. As previous studies conducted by Christian Fellinger [43] have shown, CHARMM force fields were not ideal for this application, as arginine clustered during the simulations. However, AMBER [44] force field showed promising results as shown by Dominik Sader in his Bachelor Thesis. Therefore, the AMBER-ff14SB [45] force field was used. However, the classic protein force field lacks parameters for zwitterionic amino acids. They were added manually to the existing protein force field AMBER-ff14SB parameter files in OpenMM. The required charges were obtained using ACPYPE [42]. The atom charges of the amino acids are listed in table 3.4. The atom names of the amino acids are depicted in figure 3.1. The atom names are according to AMBER-ff14SB. Angle and Bond parameters as well as atom types were assessed according to AMBER-ff14SB.

A comparison of the different force fields and water models and their influence on the dielectric spectra are depicted in figure 3.2. The AMBER force field shows better agreement than the CHARMM force field with the experimental spectrum especially in the low frequency region. The SPCE water model shows best agreement with experimental data, TIP3P and TIP3PFB (force balanced TIP3P) model are too fast and too slow, respectively and both have a higher permittivity compared to experimental data. That is why the SPCE water model was chosen in this Master's Thesis.

3.1.2 Force field optimization

Using AMBER force fields in OpenMM, the parameter of simple ions are coupled to the water model in use. As SPCE water showed the most promising results regarding

Table 3.1: Packing numbers, box size after equilibration and resulting concentration of all arginine systems with SPCE water and the optimized force field.

Salt	Expected c(salt) [M]	N(arginine)	N(water)	N(salt)
No salt	0	59	6804	0
KBr	0.15	59	6754	20
	0.30	59	6710	39
	0.45	59	6661	59
	0.60	59	6617	78
	0.75	59	6570	98
	0.90	59	6524	117
KCl	0.15	59	6750	20
	0.30	59	6702	39
	0.45	59	6648	59
	0.60	59	6600	78
	0.75	59	6549	98
	0.90	59	6498	117
KI	0.15	59	6743	20
	0.30	59	6689	39
	0.45	59	6629	59
	0.60	59	6575	78
	0.75	59	6518	98
	0.90	59	6460	117
LiCl	0.15	59	6779	20
	0.30	59	6760	39
	0.45	59	6734	59
	0.60	59	6715	78
	0.75	59	6693	98
	0.90	59	6671	117
NaCl	0.15	59	6772	20
	0.30	59	6745	39
	0.45	59	6713	59
	0.60	59	6687	78
	0.75	59	6658	98
	0.90	59	6629	117

Table 3.2: Packing numbers, box size after equilibration and resulting concentration of all lysine systems with SPCE water and the optimized force field.

Salt	Expected c(salt) [M]	N(lysine)	N(water)	N(salt)
No salt	0	130	6389	0
KBr	0.25	130	6311	33
	0.50	130	6233	65
	0.75	130	6156	98
	1.0	130	6078	130
	1.5	130	5922	195
	2.0	130	5766	260
KCl	0.25	130	6304	33
	0.50	130	6219	65
	0.75	130	6134	98
	1.0	130	6049	130
	1.5	130	5880	195
	2.0	130	5710	260
KI	0.25	130	6294	33
	0.50	130	6198	65
	0.75	130	6103	98
	1.0	130	6007	130
	1.5	130	5816	195
	2.0	130	5625	260
LiCl	0.25	130	6352	33
	0.50	130	6315	65
	0.75	130	6279	98
	1.0	130	6242	130
	1.5	130	6168	195
	2.0	130	6094	260
NaCl	0.25	130	6340	33
	0.50	130	6292	65
	0.75	130	6243	98
	1.0	130	6194	130
	1.5	130	6097	195
	2.0	130	6000	260

Table 3.3: Packing numbers, box size after equilibration of all serine systems with SPCE water and the optimized force field.

Salt	Expected c(salt) [M]	N(serine)	N(water)	N(salt)
No salt	0	130	6706	0
KBr	0.25	130	6628	33
	0.50	130	6550	65
	0.75	130	6472	98
	1.0	130	6394	130
	1.5	130	6238	195
	2.0	130	6083	260
KCl	0.25	130	6621	33
	0.50	130	6536	65
	0.75	130	6451	98
	1.0	130	6366	130
	1.5	130	6196	195
	2.0	130	6026	260
KI	0.25	130	6610	33
	0.50	130	6515	65
	0.75	130	6419	98
	1.0	130	6324	130
	1.5	130	6133	195
	2.0	130	5942	260
LiCl	0.25	130	6669	33
	0.50	130	6632	65
	0.75	130	6595	98
	1.0	130	6558	130
	1.5	130	6485	195
	2.0	130	6411	260
NaCl	0.25	130	6657	33
	0.50	130	6608	65
	0.75	130	6560	98
	1.0	130	6511	130
	1.5	130	6414	195
	2.0	130	6316	260

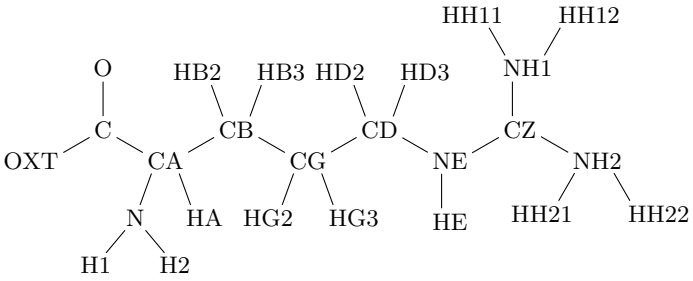

(a) Arginine

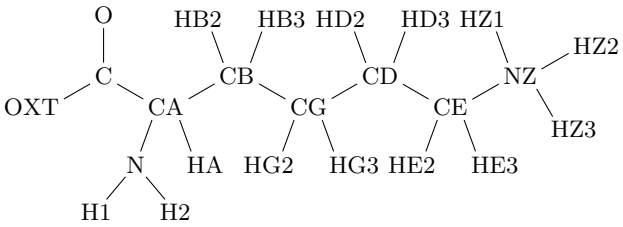

(b) Lysine

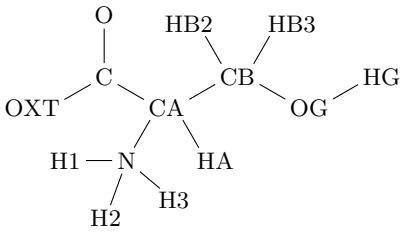

(c) Serine

Figure 3.1: Atom names of the zwitterionic amino acids under investigation.

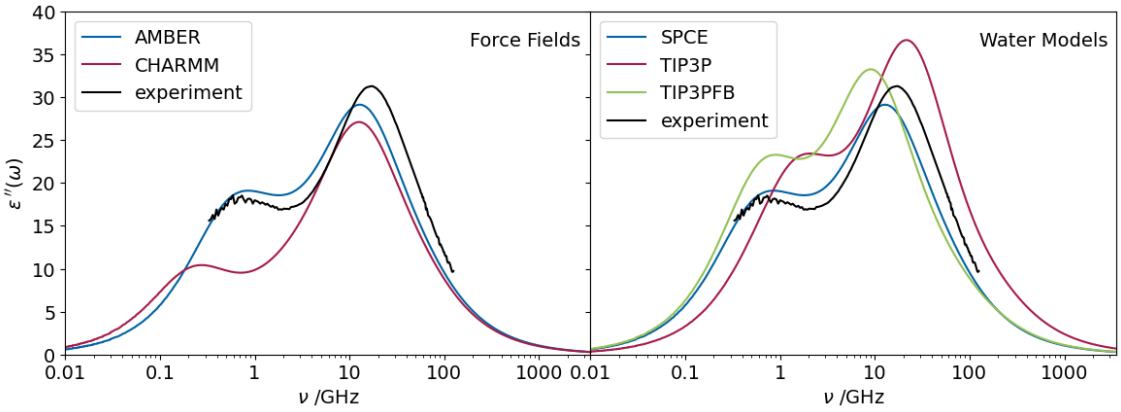

Figure 3.2: Comparison of the experimental spectrum and the calculated spectra influenced by different force fields (left) and water models (right) on the example of 0.45 M arginine, 0.45 M KCl aqueous solution.

Table 3.4: Charges generated from ACPYPE.

Arginine		Lysine		Serine	
Atom	Charge [e]	Atom	Charge [e]	Atom	Charge [e]
C	0.8666	C	0.8896	C	0.9396
O	-0.8623	O	-0.8183	O	-0.7543
OXT	-0.8623	OXT	-0.8183	OXT	-0.7543
N	-0.8838	N	-0.8988	N	-0.8276
H1	0.3418	H1	0.3478	H1	0.4478
H2	0.3418	H2	0.3475	H2	0.4478
				H3	0.4478
CA	0.0615	CA	0.0155	CA	-0.1135
HA	0.0757	HA	0.0177	HA	0.0897
CB	-0.0734	CB	-0.0574	CB	0.1164
HB2	0.0552	HB2	0.0192	HB2	0.0892
HB3	0.0552	HB3	0.0192	HB3	0.0892
CG	-0.0904	CG	-0.0944	OG	-0.6308
HG2	0.0557	HG2	0.0557	HG	0.4130
HG3	0.0557	HG3	0.0557		
CD	-0.0057	CD	-0.1524		
HD2	0.0627	HD2	0.1217		
HD3	0.0627	HD3	0.1217		
NE	-0.3561	CE	0.1148		
HE	0.3007	HE2	0.1052		
CZ	0.5253	HE3	0.1052		
NH1	-0.4552	NZ	-0.8466		
HH11	0.29545	HZ1	0.4498		
HH12	0.29545	HZ2	0.4498		
NH2	-0.4552	HZ3	0.4498		
HH21	0.29545				
HH22	0.29545				

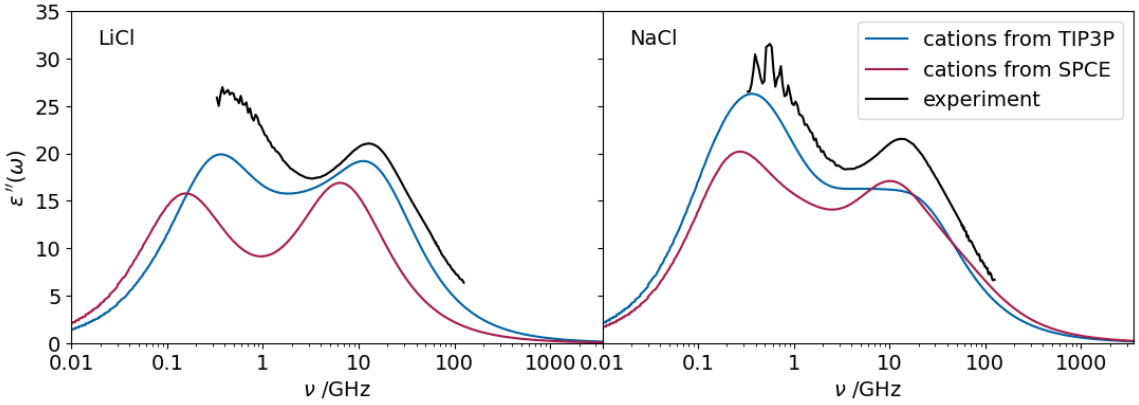

Figure 3.3: Comparison of the spectra with different ion parameters on the example of 1.0 M lysine. The left side shows the spectra with different parameters for Li^+ in 2 M LiCl, the right side for different parameters for Na^+ in 2 M NaCl.

the dielectric behavior of water, the parameters of SPCE was taken. However, at high concentrations of lithium and sodium the agreement of computed spectra and experimental spectra decreased, which is why the cation parameter used for all simulations were taken from the ion parameter for the TIP3P water model. Figure 3.3 shows the spectra using different cation parameters.

3.2 Analysis

The trajectories were analyzed using the MDAnalysis package [46] with added functions of an in house package.

3.2.1 Calculation of dielectric spectra

The spectra were calculated using the in house package GENDICON [26]. As the simulations were all non-polarizable and all charged species are represented by soft spheres, the ionic species do not have a dipole moment and do not contribute to M_D. Additionally, the ions are solvatized and the time correlation function (Φ) including the collective translational dipole moment M_J is negligible. The ions contribute to the static conductivity σ. The rotating dipole moment M_D, attributed to water and the respective amino acid, is the only relevant property in this work to calculate the dielectric spectra.

One important task is to decompose the time correlation function (TCF) in a meaningful manner. In this work the total dipole moment of one molecular species was correlated to the total dipole moment to obtain one TCF for each molecular species.

$$\Phi_{tot} = \langle M_D^{aa} \cdot M_D^{tot} \rangle + \langle M_D^{water} \cdot M_D^{tot} \rangle = \langle M_D^{tot} \cdot M_D^{tot} \rangle \tag{3.1}$$

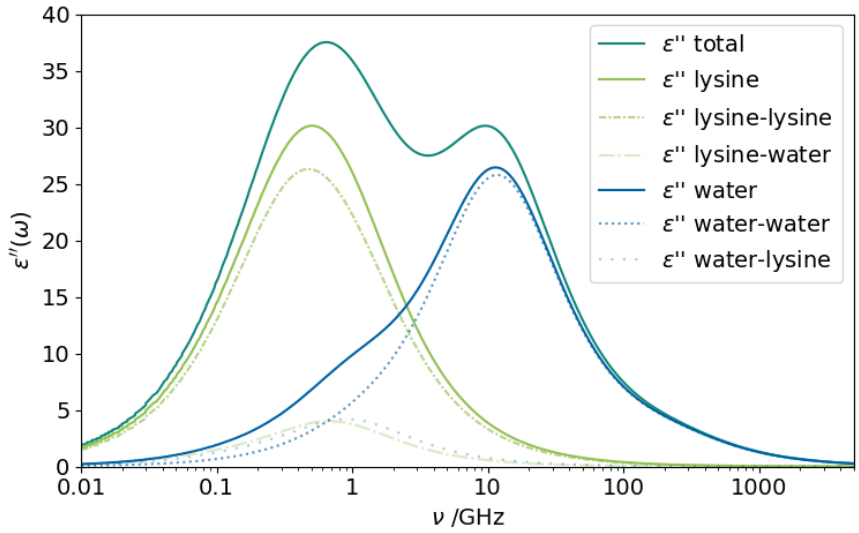

Figure 3.4: Decomposition of the spectra in terms of cross and self terms calculated from the auto and cross correlations of the species lysine and water.

Another possible decomposition is to calculate each term, self terms and cross terms for each molecular species:

$$\Phi_{tot} = \langle M_D^{aa} \cdot M_D^{aa} \rangle + \langle M_D^{aa} \cdot M_D^{water} \rangle + \langle M_D^{water} \cdot M_D^{aa} \rangle + \langle M_D^{water} \cdot M_D^{water} \rangle = \langle M_D^{tot} \cdot M_D^{tot} \rangle \tag{3.2}$$

Where $\langle M_D^{aa} \cdot M_D^{water} \rangle$ is equal to $\langle M_D^{water} \cdot M_D^{aa} \rangle$ if there is sufficient data. Figure 3.4 shows the decomposition in cross correlations and auto correlations on the example of 1 M lysine in water with no salt added. In this case the cross terms do not have a perfect overlap which is due to statistical errors. The ergodic hypothesis states that simulations of small systems for a period of time yields time-averaged molecular properties that approach the experimentally measurable ensemble averages [47]. Limited data yields results that might not represent experimental data. As the cross terms are not relevant in this work, the decomposition according to eq. 3.1 was chosen.

3.3 Experimental data

The experimental data is from our collaborators from Max Planck institute for polymer research in Mainz, Johannes Hunger and Vasileios Balos. In total two measurement took place, one in 2021 and one in 2023, referred to as old experimental data and new experimental data. The old experimental data includes measurements of 0.45 M arginine, 1 M lysine and 1 M serine with KBr, KCl, KI, LiCl and NaCl at concentrations of 0, 0.15, 0.30, 0.45, 0.60, 0.75 and 0.90 M in the case of arginine and 0, 0.25, 0.50, 0.75,

1.0, 1.5, 2.0 M in the case of lysine and serine. The new experimental data includes measurements of 0.45 M arginine, 1 M lysine and 1 M serine with KCl, KI, LiCl and NaCl at concentrations of 0, 0.20, 0.40, 0.60, 0.80 and 1.0 M in the case of arginine and 0, 0.25, 0.50, 0.75, 1.0, 1.5, 2.0 M in the case of lysine and serine. Due to KBr not being included in the measurements and the concentrations of the other salts being different in the case of arginine, only the data from old experiments is used for the comparison of the dielectric spectra in the case of arginine. For comparison of the other amino acids the new experimental data is taken as reference for the dielectric spectra, except in the case of KBr as it was not measured the second time. The trends of the dielectric spectra were all taken from the new measurements, as they are more accurate and they don't need to have the same concentrations as the computed spectra to be used for comparison.

4 Results and discussion

4.1 State of research

Previous work on the dielectric behavior of arginine in different electrolyte solutions [43] showed that working with CHARMM force fields led to arginine cluster formation. Therefore, the arginine peaks were shifted to lower frequency than suggested by experimental data. Changing the force field to AMBER force fields showed promising results in the Bachelor's Thesis of Dominik Sader.

Figure 4.1 shows the comparison of force fields and water models on the example of 0.45 M KBr and 0.45 M arginine solutions. The experimental spectrum is represented by the black line and used as reference. When CHARMM force fields were used for simulations, the arginine molecules aggregated in clusters which can be seen as a shift to lower frequencies in the red and orange spectra. The spectrum in orange used a CHARMM force field with a scaling of 1.1 on the van der Waals interactions between the oxygen of water and all atoms of arginine [43]. The red spectrum used a similar scaling of 1.2 to increase the water-amino acid interaction even further. However, higher scaling

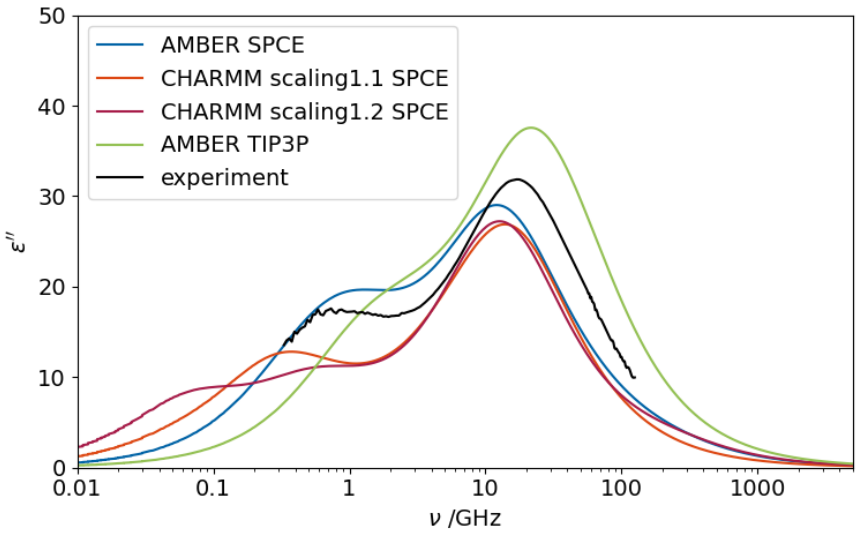

Figure 4.1: Comparison of the spectra from previous work (orange, red and green) and this work (blue) with the experimental spectrum (black) on the example of 0.45 M KBr and 0.45 M arginine.

did not improve the agreement of the computed spectra with the experimental spectra in all tested electrolyte solutions [43], as can be seen in this example. A new approach with AMBER force fields was used in the Bachelor's Thesis of Dominik Sader (green line). The peak at lower frequencies, attributed to arginine, shows better agreement than CHARMM force fields. However, the TIP3P water model was used, which leads to the water peak being more intense and an overall shift to higher frequencies. TIP3P water has a lower viscosity than water shows in experiments [48, 49]. Therefore, the rotation of the water molecules are faster in TIP3P water which leads to a shift to higher frequencies. In blue is the spectrum from this work, using an optimized force field consisting of AMBER force fields and the SPCE water model with cation parameters from the TIP3P water model. The spectrum calculated using the optimized force field parameters shows the best agreement with experimental data.

4.2 Dielectric spectra

All calculated spectra are the average spectra of five replica. The real part of the total spectrum is depicted in orange, contributions from amino acids are red and contributions from water are yellow. The imaginary part of the total spectrum is depicted in turquoise, contributions from amino acids are green and contributions from water are blue. The real part of the experimental spectra is depicted in gray and the imaginary part in black. The amino acid concentration is constant in all spectra, 0.45 M in the case of arginine and 1 M in the case of serine and lysine.

The relative dielectric permittivity of the respective amino acid and water decreases with increasing salt concentration. This effect is called the dielectric decrement. It is visible is all examined electrolyte solutions. The extent of the decrease and the dependence on the salt concentration is thoroughly discussed in section 4.2.4.

The dielectric spectra were all calculated with equation 2.24 which is why only species with a permanent dipole contribute to the computed spectra. This is a simplification as ion pairs also contribute to dielectric spectra. However, their contribution is usually small due to weak binding between ion pairs [50]. The ion pairs show a contribution to the dielectric spectra at low frequencies at around 1 GHZ [8]. In this Master's Thesis the ion pair contributions were neglected due to their small contribution to the total dielectric spectrum and as the focus was on the change of the dielectric properties of amino acids due to different salts of the Hofmeister series rather than the dielectric properties of those salts in solution themselves.

4.2.1 Arginine

The calculated spectrum of 0.45 M arginine in water with no salt added is shown in figure 4.2. The top graph shows the imaginary part of the spectrum. The computed contribution of arginine (green) and the computed contribution of water (blue) are close to the experimental values for arginine (black dash-dotted line) and water (black dotted line). The total spectrum is the sum of the two contributions (turquoise) and shows

good agreement with the experimental data (solid black line). The molecular species arginine and water contribute one peak each when the correlation functions are evaluated according to equation 3.1. The peak at lower frequencies is attributed to arginine, the one at higher frequencies to water. The experimental data used in the plot is from the new experiment. The bottom graph shows the real part of the spectrum. The contribution of arginine is shown in red, the contribution of water in yellow. Similar to the imaginary part, the total spectrum is the sum of the contributions and in orange. The total spectrum shows two points of inflections, at the position of the peak maxima in the imaginary part. The real part also shows good agreement to the experimental data.

The calculated and experimental spectra of 0.45 M arginine and KBr, KCl, KI, LiCl and NaCl are shown in figure 4.3, 4.4, 4.5, 4.6 and 4.7, respectively. The spectra used for comparison are taken from the old experiment due to the concentrations of the new data differing from the concentrations the simulations were made with. Overall, the agreement of the experimental and computed spectra is good. Closer inspection shows that the arginine peak is overestimated at lower salt concentrations. Additionally, the water peak is slightly shifted to lower frequencies and is less intense than experimentally, which is visible in all spectra, also from other amino acids and is due to the SPCE water model as similar results have been reported [51].

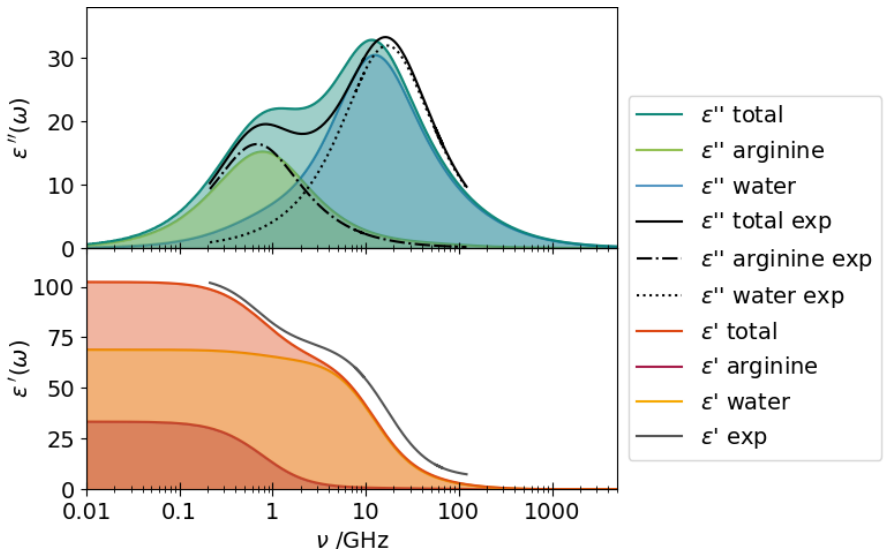

Figure 4.2: Imaginary ($\varepsilon''(\omega)$) and real ($\varepsilon'(\omega)$) part of the dielectric spectra of 0.45 M arginine in water with no salt added.

Potassium bromide

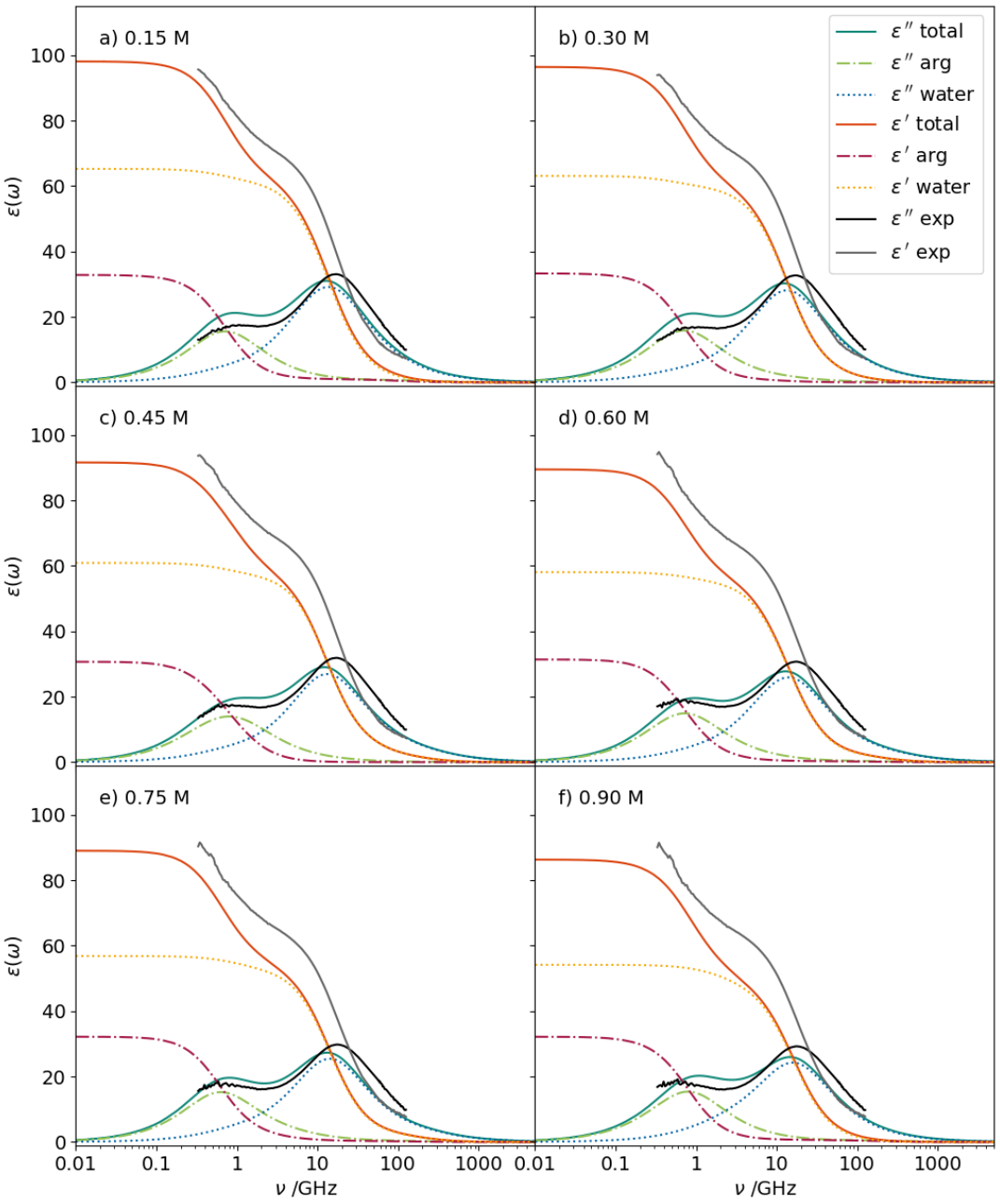

Figure 4.3: Dielectric spectra of arginine and KBr with a concentration of a) 0.15 M, b) 0.30 M, c) 0.45 M, d) 0.60 M, e) 0.75 M, f) 0.90 M in SPCE water.

Potassium chloride

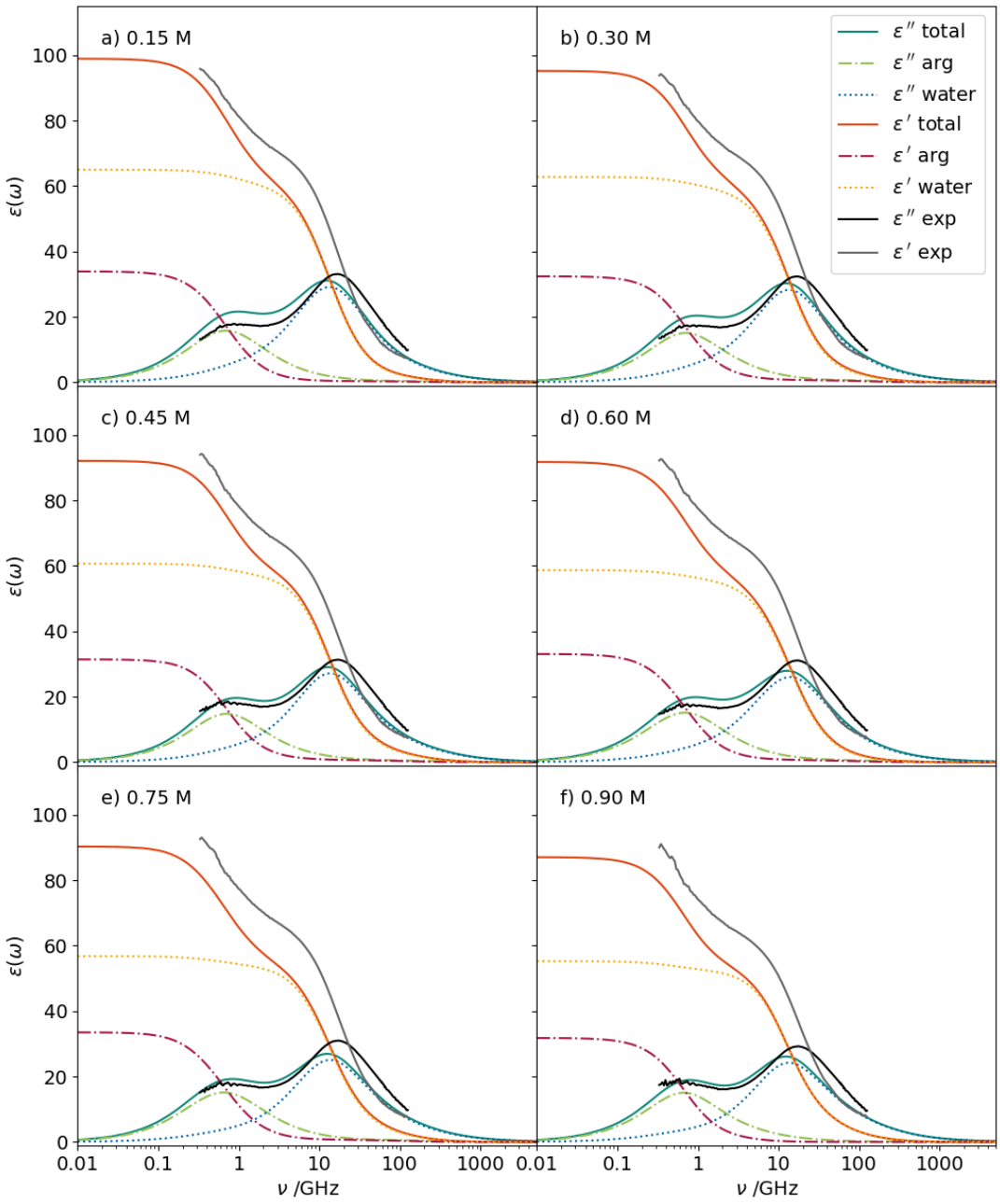

Figure 4.4: Dielectric spectra of arginine and KCl with a concentration of a) 0.15 M, b) 0.30 M, c) 0.45 M, d) 0.60 M, e) 0.75 M, f) 0.90 M in SPCE water.

Potassium iodide

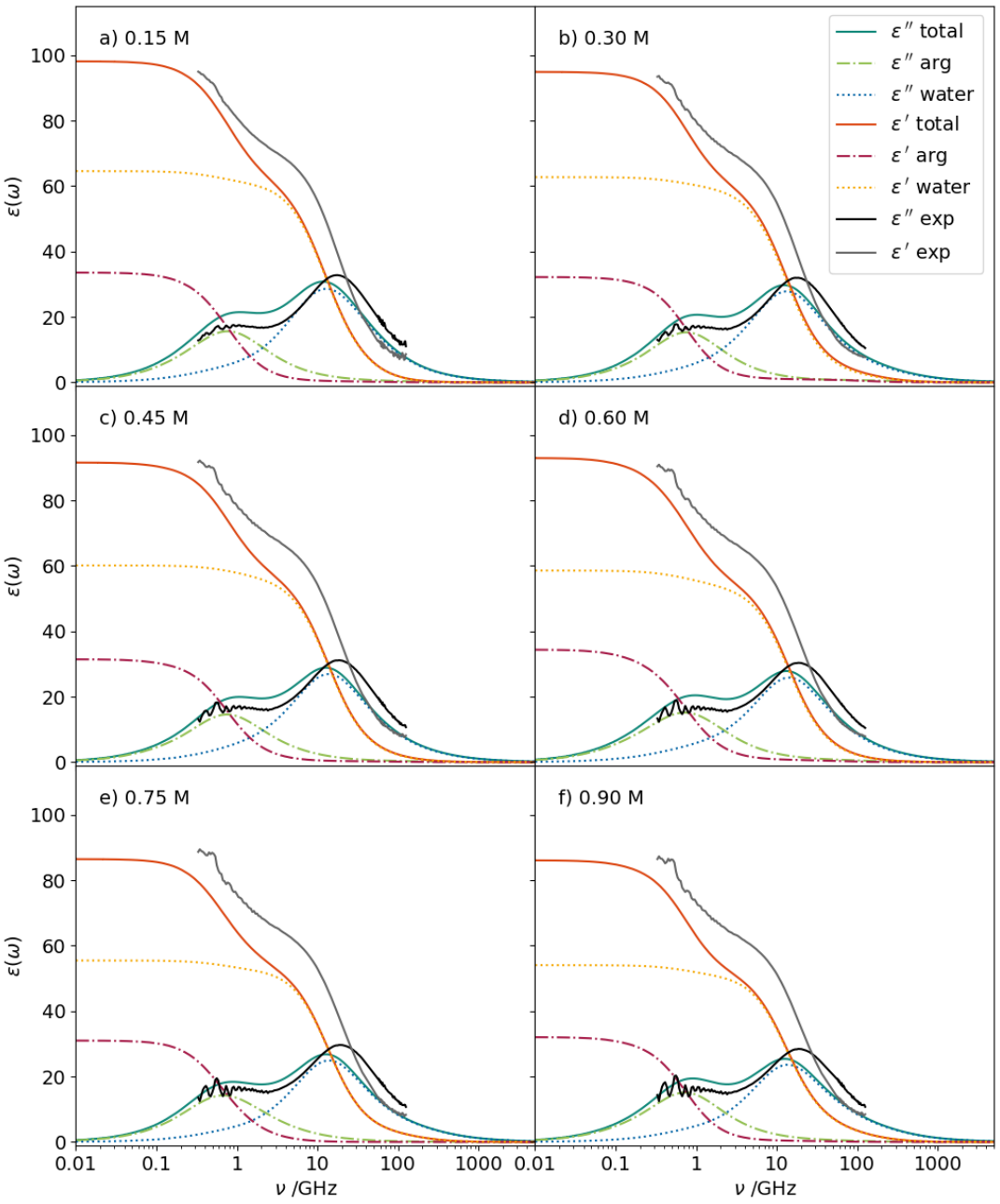

Figure 4.5: Dielectric spectra of arginine and KI with a concentration of a) 0.15 M, b) 0.30 M, c) 0.45 M, d) 0.60 M, e) 0.75 M, f) 0.90 M in SPCE water.

Lithium chloride

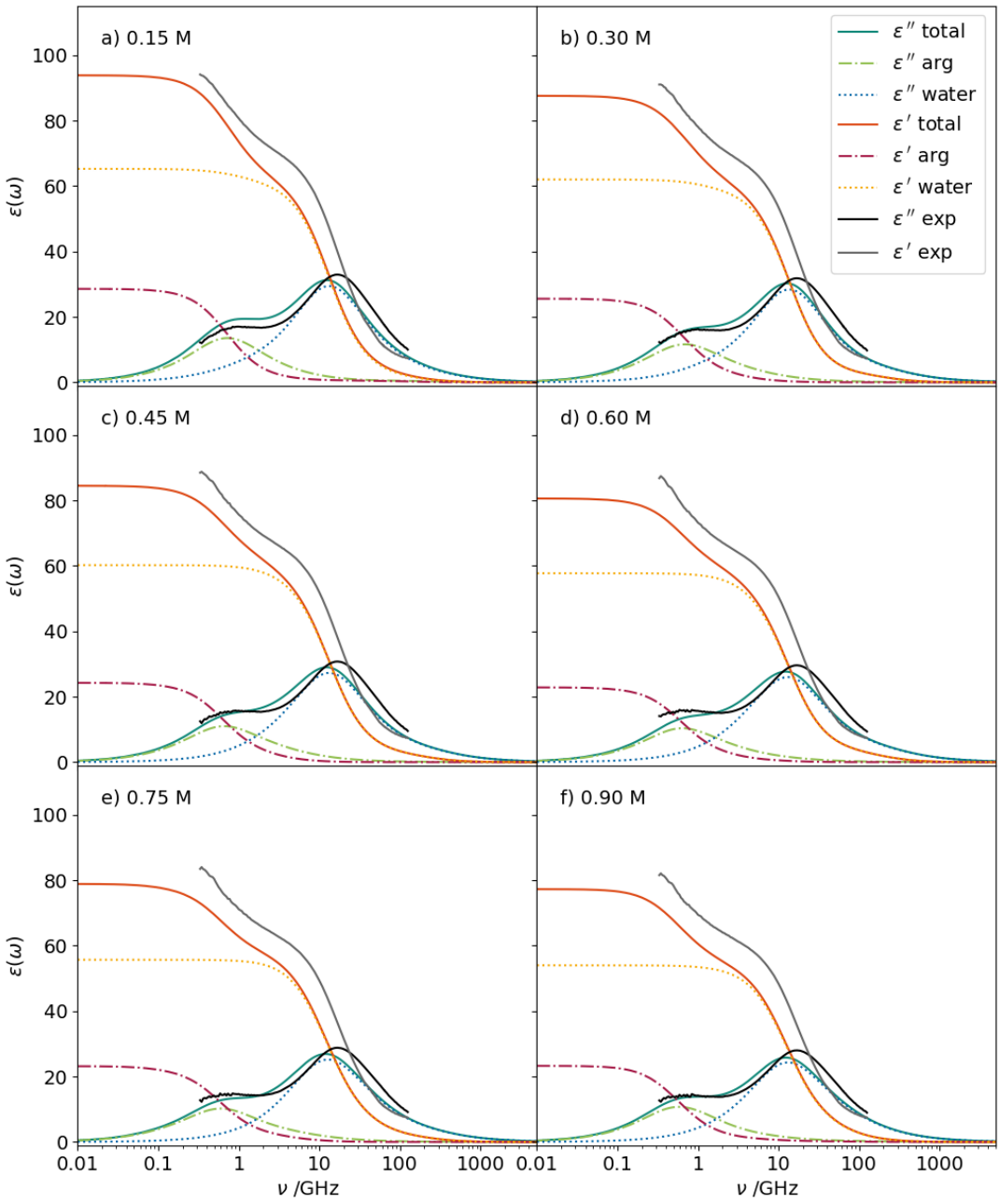

Figure 4.6: Dielectric spectra of arginine and LiCl with a concentration of a) 0.15 M, b) 0.30 M, c) 0.45 M, d) 0.60 M, e) 0.75 M, f) 0.90 M in SPCE water.

Sodium chloride

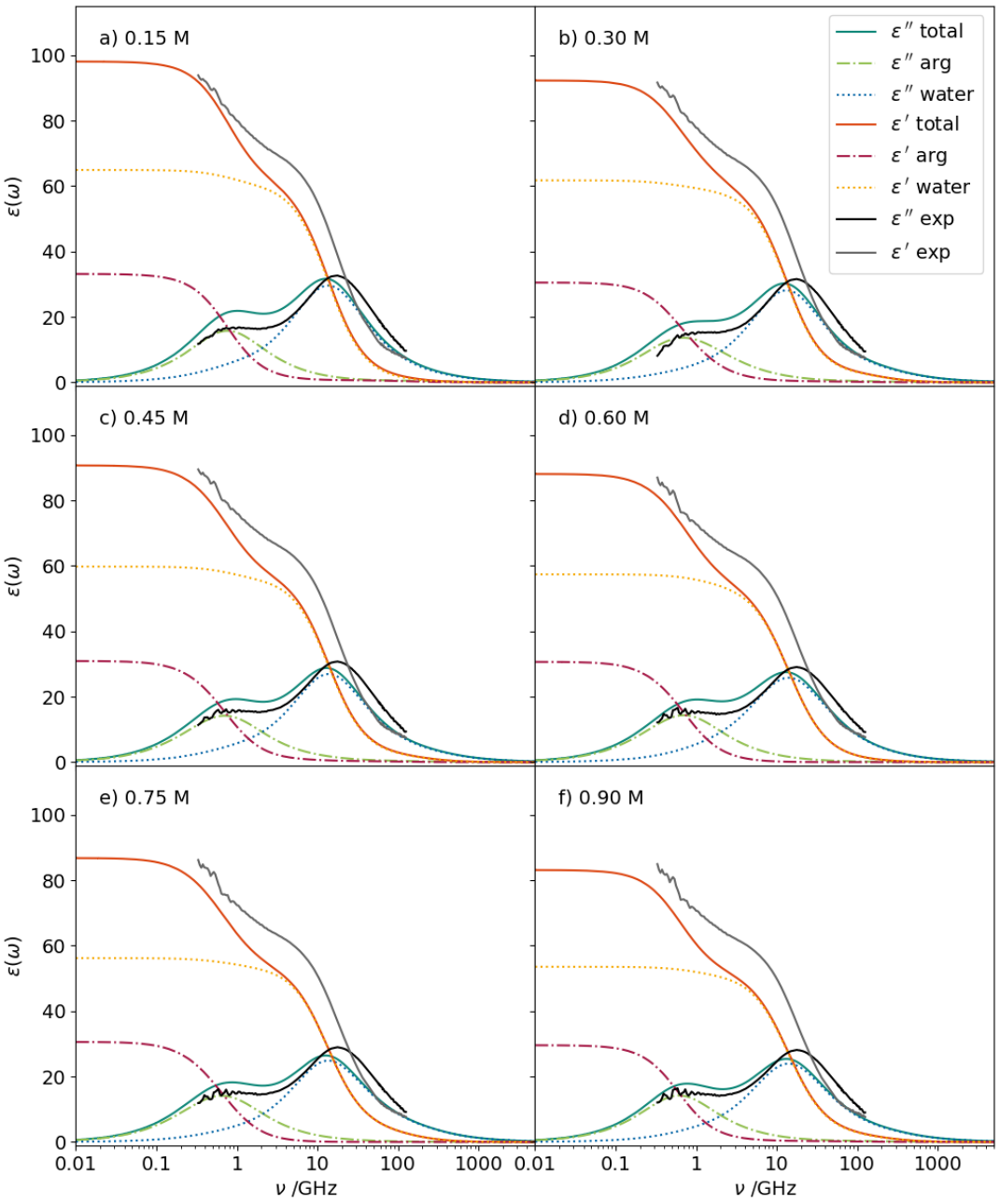

Figure 4.7: Dielectric spectra of arginine and NaCl with a concentration of a) 0.15 M, b) 0.30 M, c) 0.45 M, d) 0.60 M, e) 0.75 M, f) 0.90 M in SPCE water.

4.2.2 Lysine

The calculated spectrum of 1 M lysine in water with no salt added is shown in figure 4.8. The top graph shows the imaginary part of the spectrum. The computed spectrum (turquoise) shows good agreement with the experimental data (black). The contribution of lysine (green) and water blue has a high correspondence to the experimental data of lysine (black dash-dotted line) and water (black dotted line). The peak at lower frequencies is attributed to lysine, the one at higher frequencies to water. The lysine peak looks like one smooth peak, whereas the water peak seems to consist of two peaks. This is due to the decomposition of the time correlation function according to equation 3.1. This leads to the water and lysine peak in the spectrum consisting of one cross term and one self term each. Section 3.2.1 shows the spectrum of lysine partitioned in cross terms and auto terms in figure 3.4. The small visible bump in the water peak is caused by the cross peak at low frequencies. The lysine peak overlaps the cross peak which is why it is not visible in the total lysine peak. This is also the reason for the deviation from the experimental peak, as the experimenters assumed the peak shape of the water peak to correspond to one Cole-Cole relaxation process, which leads to broadened but symmetric peaks. The bottom graph shows the real part of the spectrum. The contribution of lysine is shown in red, the contribution of water in yellow. Similar to the imaginary part, the total spectrum is the sum of the contributions and is depicted in orange.

The calculated and experimental spectra of 1.0 M lysine and KBr, KCl, KI, LiCl and NaCl are shown in figure 4.9, 4.10, 4.11, 4.12 and 4.13, respectively. The experimental data in all figures but figure 4.9 are from the new experiment. The lysine peak of the computed spectra tend to be shifted to lower frequencies compared to the experimental spectra. However, the overall agreement is very good.

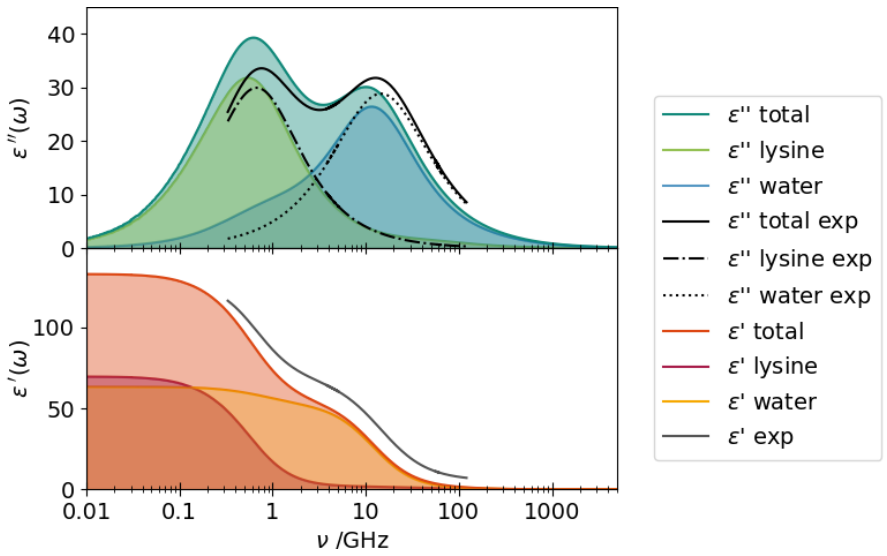

Figure 4.8: Imaginary ($\varepsilon''(\omega)$) and real ($\varepsilon'(\omega)$) part of the dielectric spectra of 1 M lysine in water with no salt added.

Potassium bromide

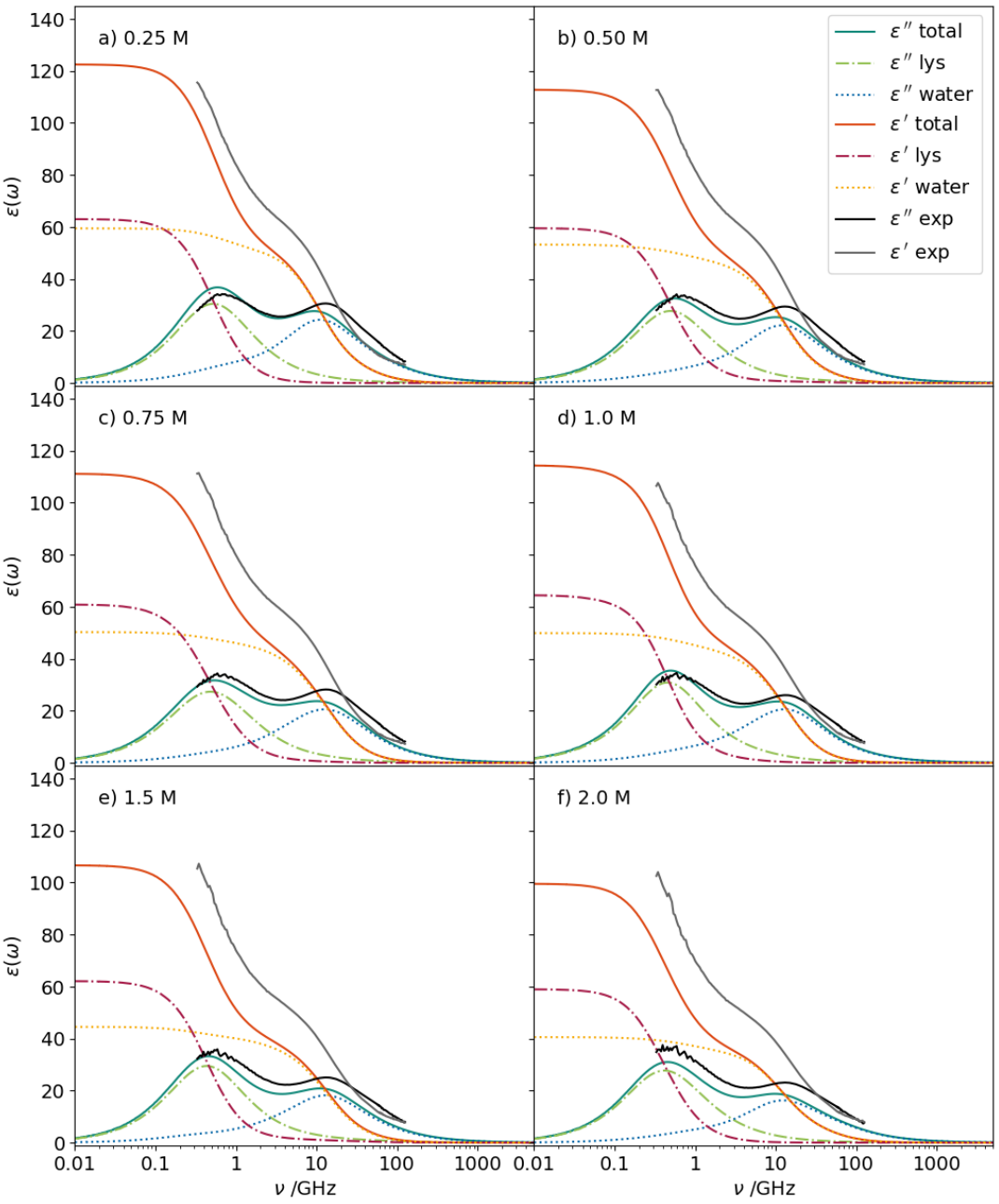

Figure 4.9: Dielectric spectra of lysine and KBr with a concentration of a) 0.25 M, b) 0.50 M, c) 0.75 M, d) 1.0 M, e) 1.5 M, f) 2.0 M in SPCE water.

Potassium chloride

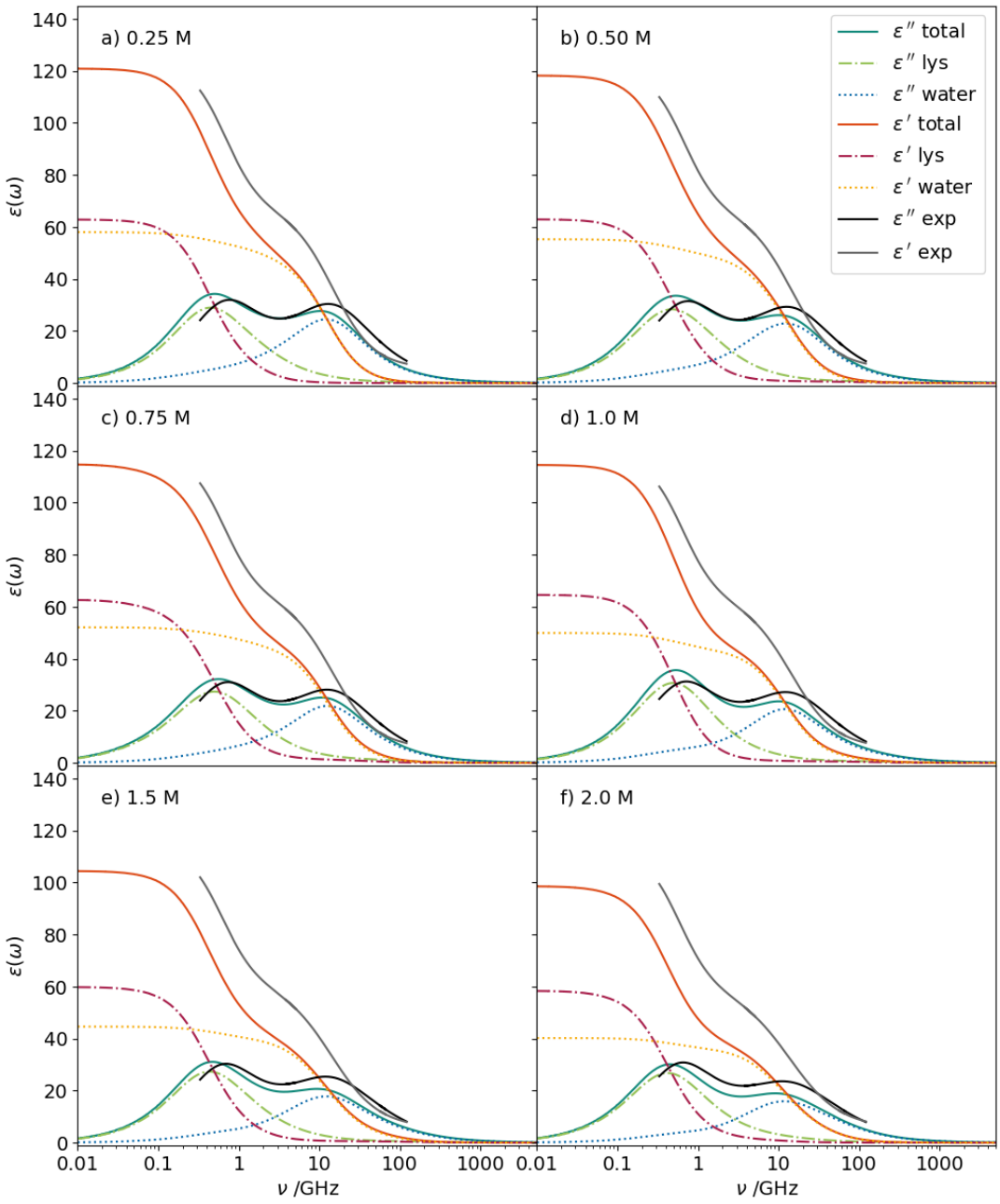

Figure 4.10: Dielectric spectra of lysine and KCl with a concentration of a) 0.25 M, b) 0.50 M, c) 0.75 M, d) 1.0 M, e) 1.5 M, f) 2.0 M in SPCE water.

Potassium iodide

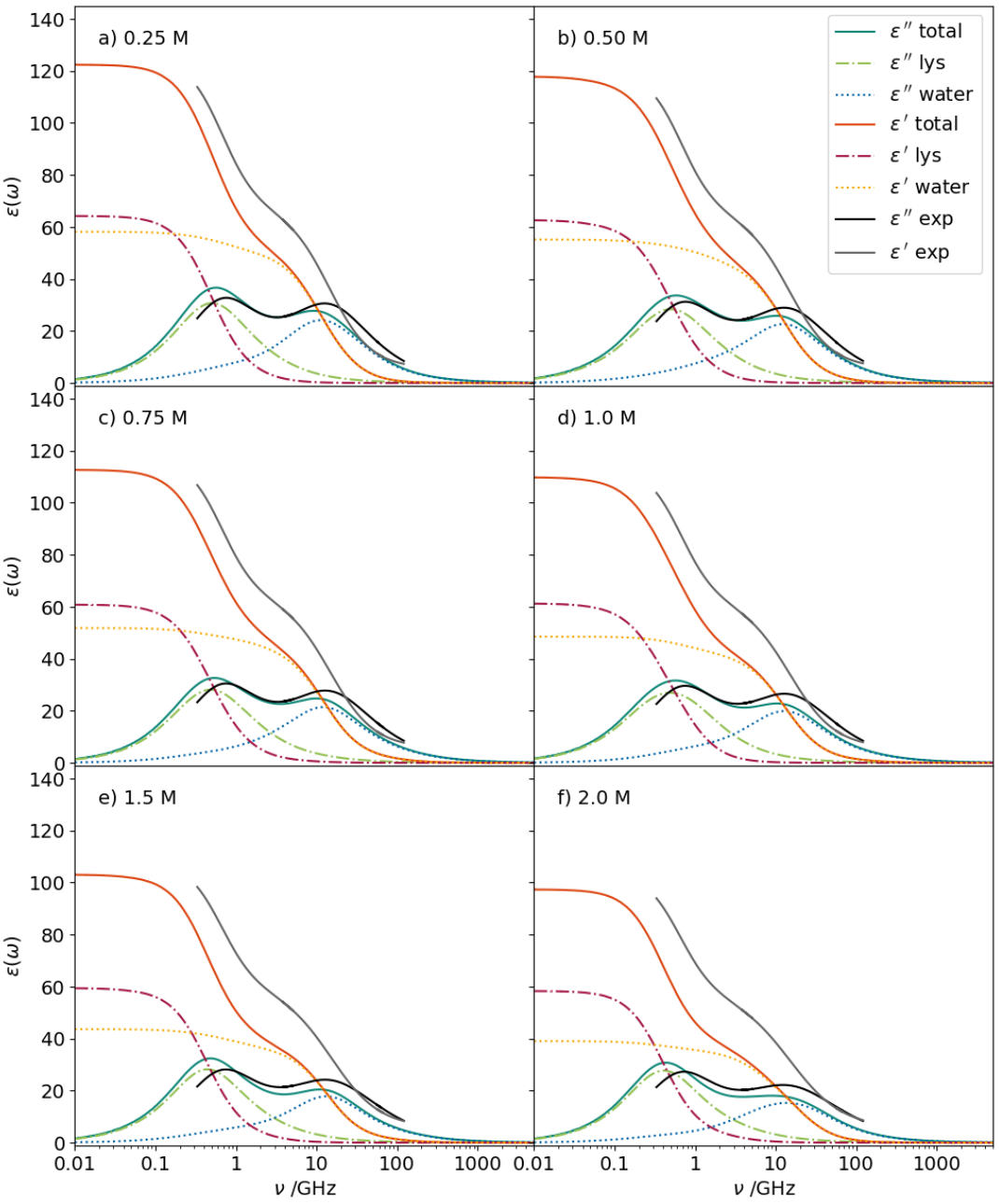

Figure 4.11: Dielectric spectra of lysine and KI with a concentration of a) 0.25 M, b) 0.50 M, c) 0.75 M, d) 1.0 M, e) 1.5 M, f) 2.0 M in SPCE water.

Lithium chloride

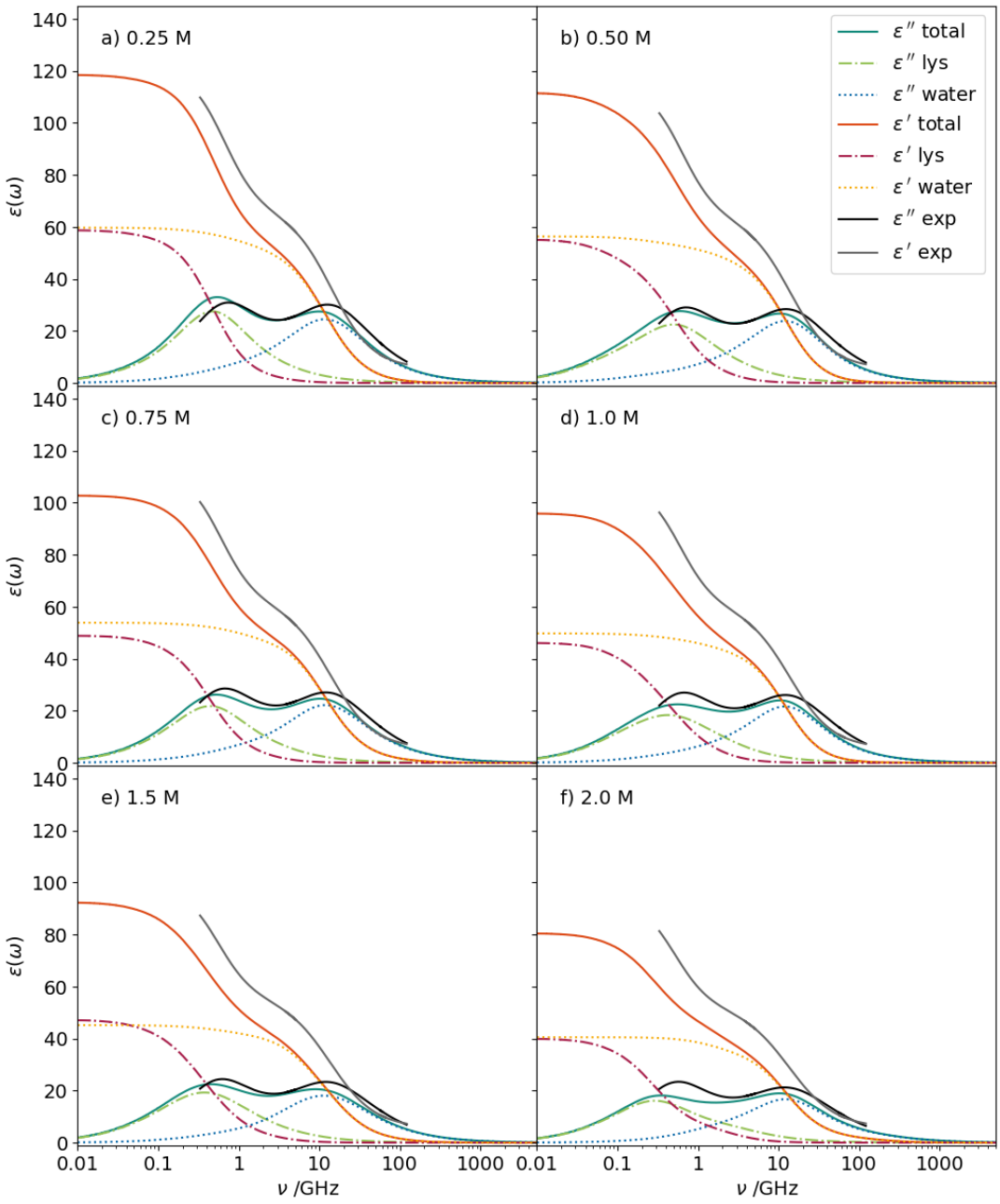

Figure 4.12: Dielectric spectra of lysine and LiCl with a concentration of a) 0.25 M, b) 0.50 M, c) 0.75 M, d) 1.0 M, e) 1.5 M, f) 2.0 M in SPCE water.

Sodium chloride

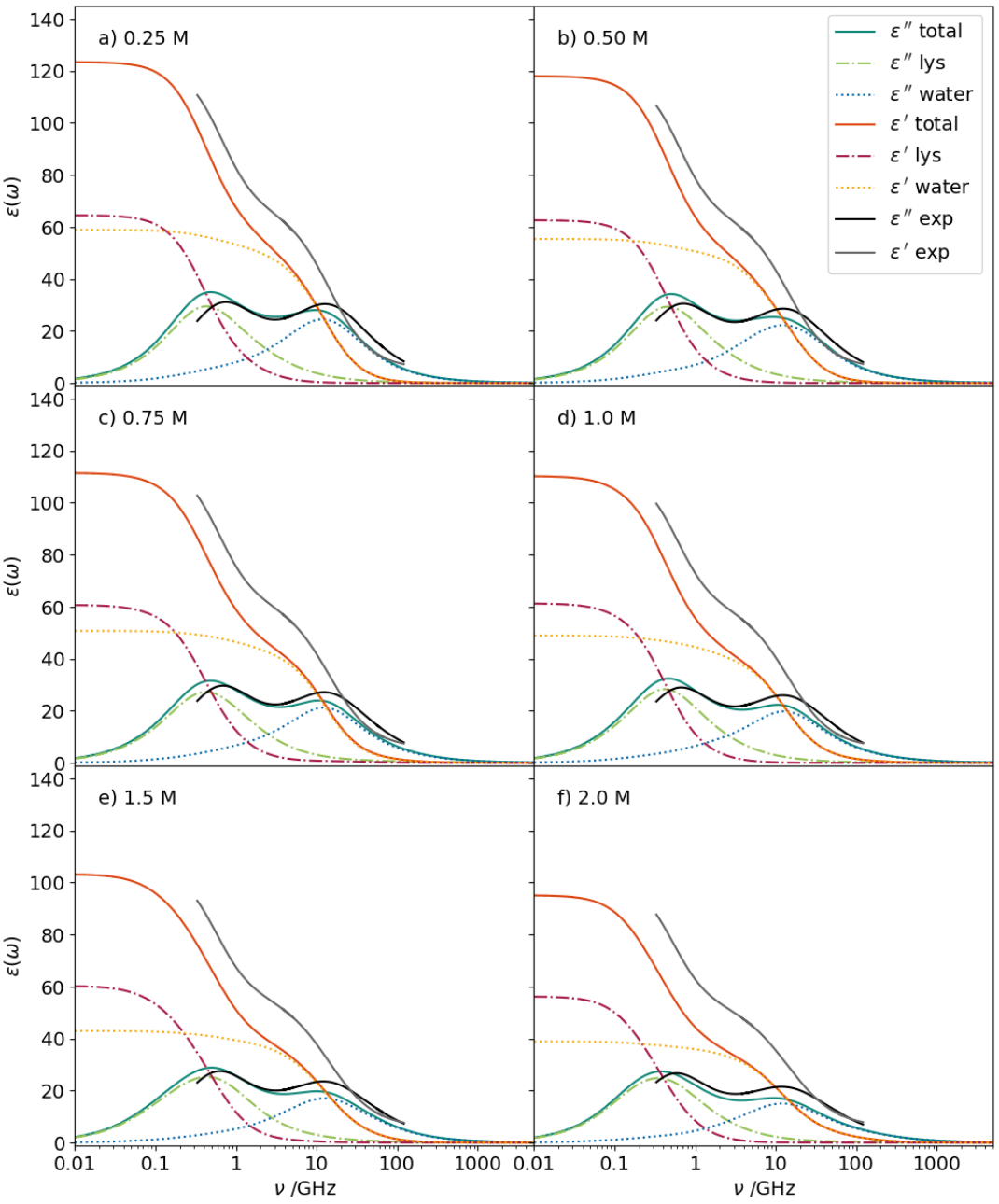

Figure 4.13: Dielectric spectra of lysine and NaCl with a concentration of a) 0.25 M, b) 0.50 M, c) 0.75 M, d) 1.0 M, e) 1.5 M, f) 2.0 M in SPCE water.

4.2.3 Serine

The spectrum of 1 M serine in water is depicted in figure 4.14. Comparing the imaginary part of the calculated and the experimental spectrum one can see that the shoulder at low frequencies is missing in the computed spectrum. This is due to the serine peak (computed in green, fitted from the experiment as dash-dotted line) being underestimated in the computational spectrum. There could be various reasons for the peak being underrepresented. The charges for the amino acids were all taken from ACPYPE and not modified to fit dielectric data. In the case of arginine and lysine the dielectric data shows good agreement but in the case of serine it does not. The intensity of the water peak and the frequencies of the peak maxima seem to fit well. Serine is still investigated without further adjustments of the force field as specific ion effects could still be observed even though the absolute values of computed and experimental data differs. The differences between computed and experimental data can also be seen in the real part of the spectrum. It can be seen that the permittivity of the experimental spectrum is higher than the permittivity of the computed spectrum but the data coming closer to an agreement at higher frequencies due to water having better agreement between computed and experimental data.

The calculated and experimental spectra of 1.0 M serine and KBr, KCl, KI, LiCl and NaCl are shown in figure 4.15, 4.16, 4.17, 4.18 and 4.19, respectively. Knowing from the serine and water spectra without salt added that the serine peak is underestimated, this inaccuracy is observable in the salt mixtures as well. Therefore, the overlap between experimental and computed data is not as good as in arginine and lysine spectra. However, there is still a strong agreement between the experimental data and the computed spectrum in the case of the water peak and the frequencies of the serine peak. Other than the intensity of the peak the experimental and computed spectra are similar.

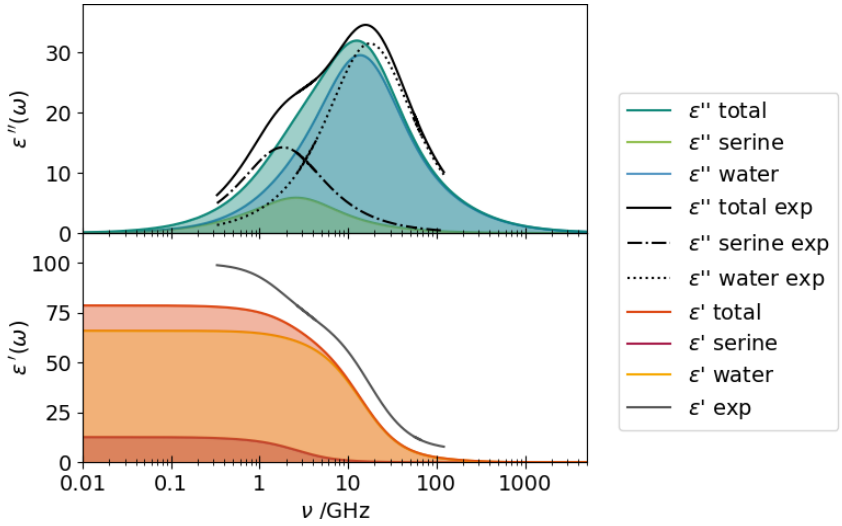

Figure 4.14: Imaginary ($\varepsilon''(\omega)$) and real ($\varepsilon'(\omega)$) part of the dielectric spectra of 1 M serine in water with no salt added.

Potassium bromide

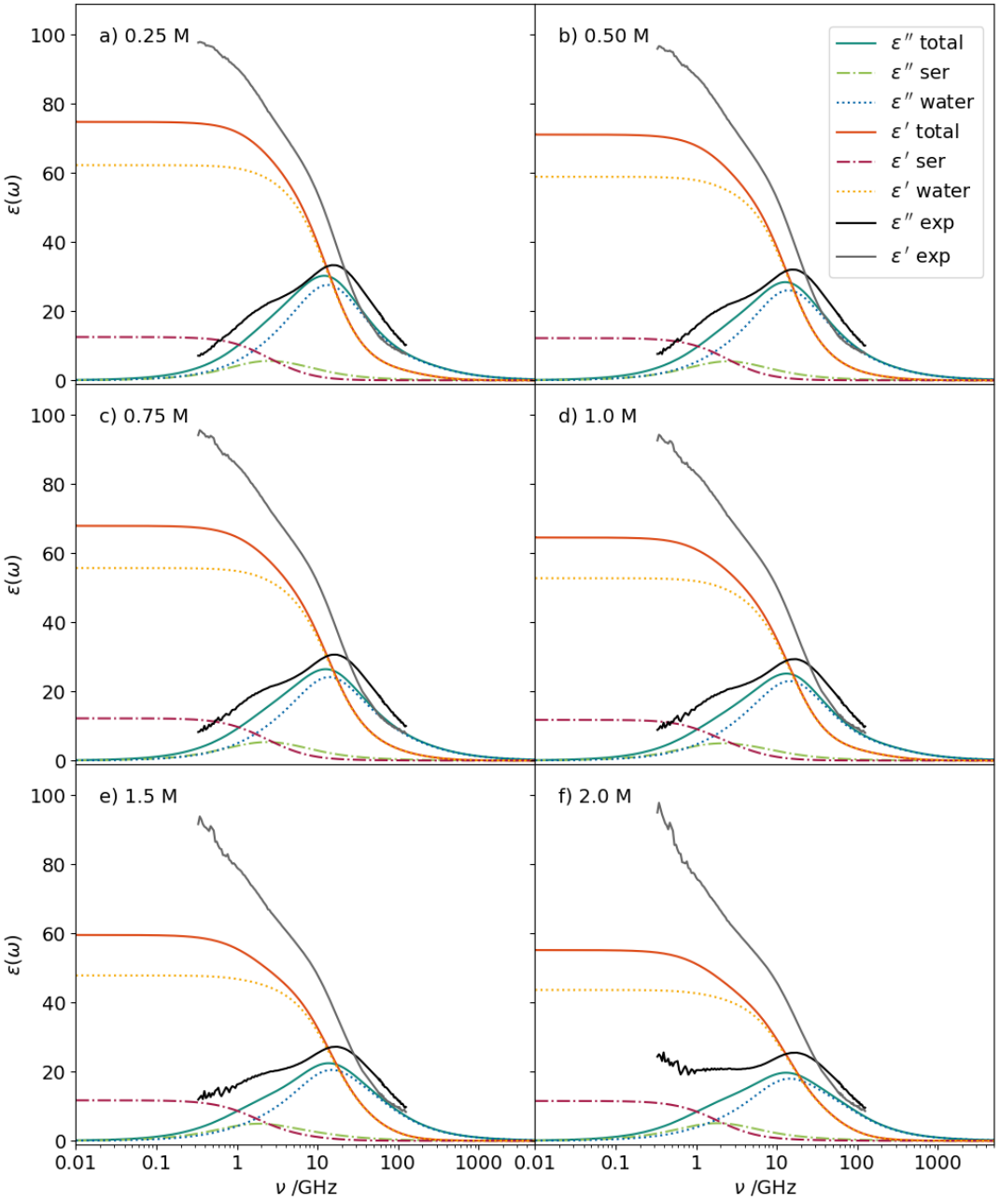

Figure 4.15: Dielectric spectra of serine and KBr with a concentration of a) 0.25 M, b) 0.50 M, c) 0.75 M, d) 1.0 M, e) 1.5 M, f) 2.0 M in SPCE water.

Potassium chloride

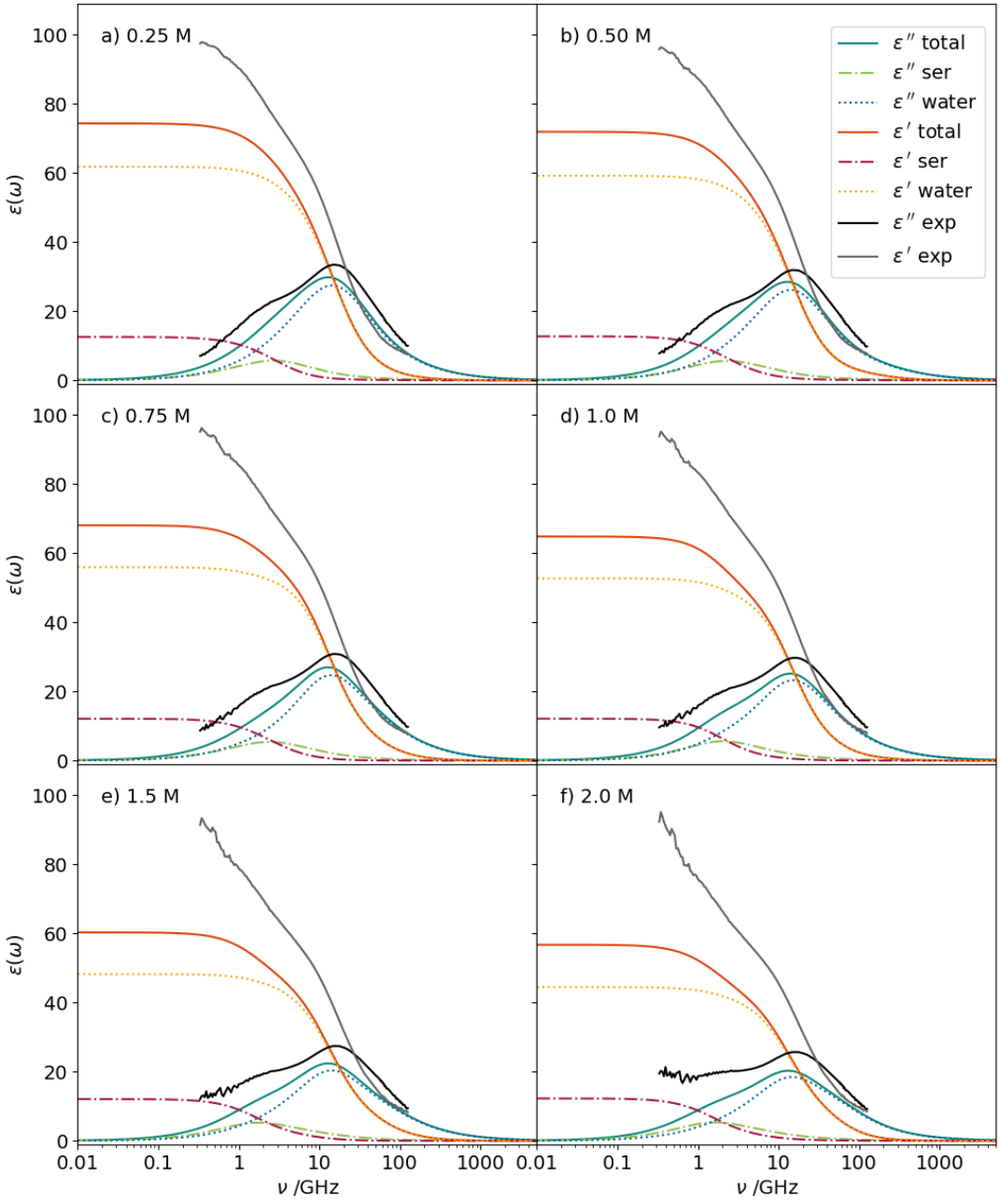

Figure 4.16: Dielectric spectra of serine and KCl with a concentration of a) 0.25 M, b) 0.50 M, c) 0.75 M, d) 1.0 M, e) 1.5 M, f) 2.0 M in SPCE water.

Potassium iodide

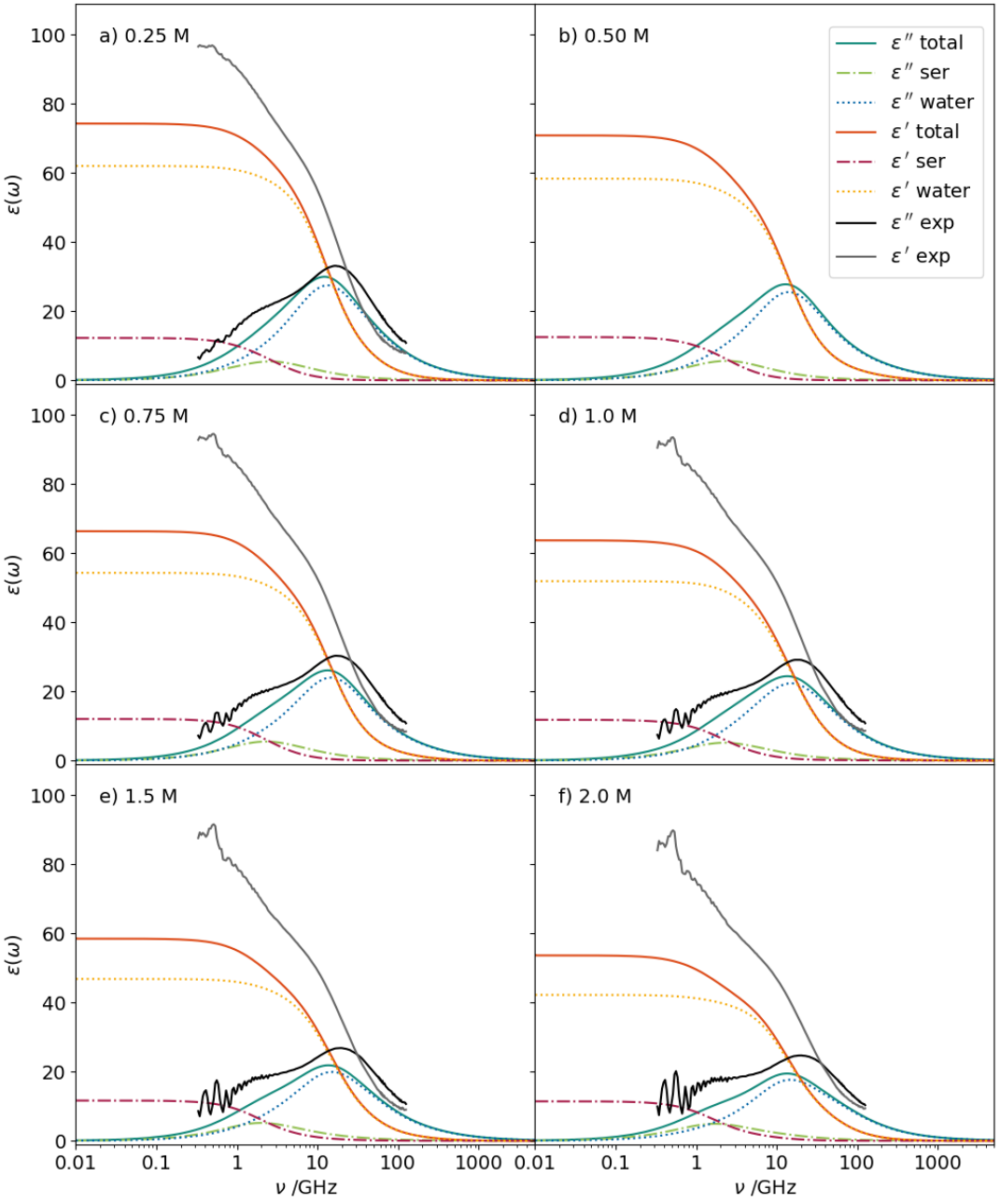

Figure 4.17: Dielectric spectra of serine and KI with a concentration of a) 0.25 M, b) 0.50 M, c) 0.75 M, d) 1.0 M, e) 1.5 M, f) 2.0 M in SPCE water.

Lithium chloride

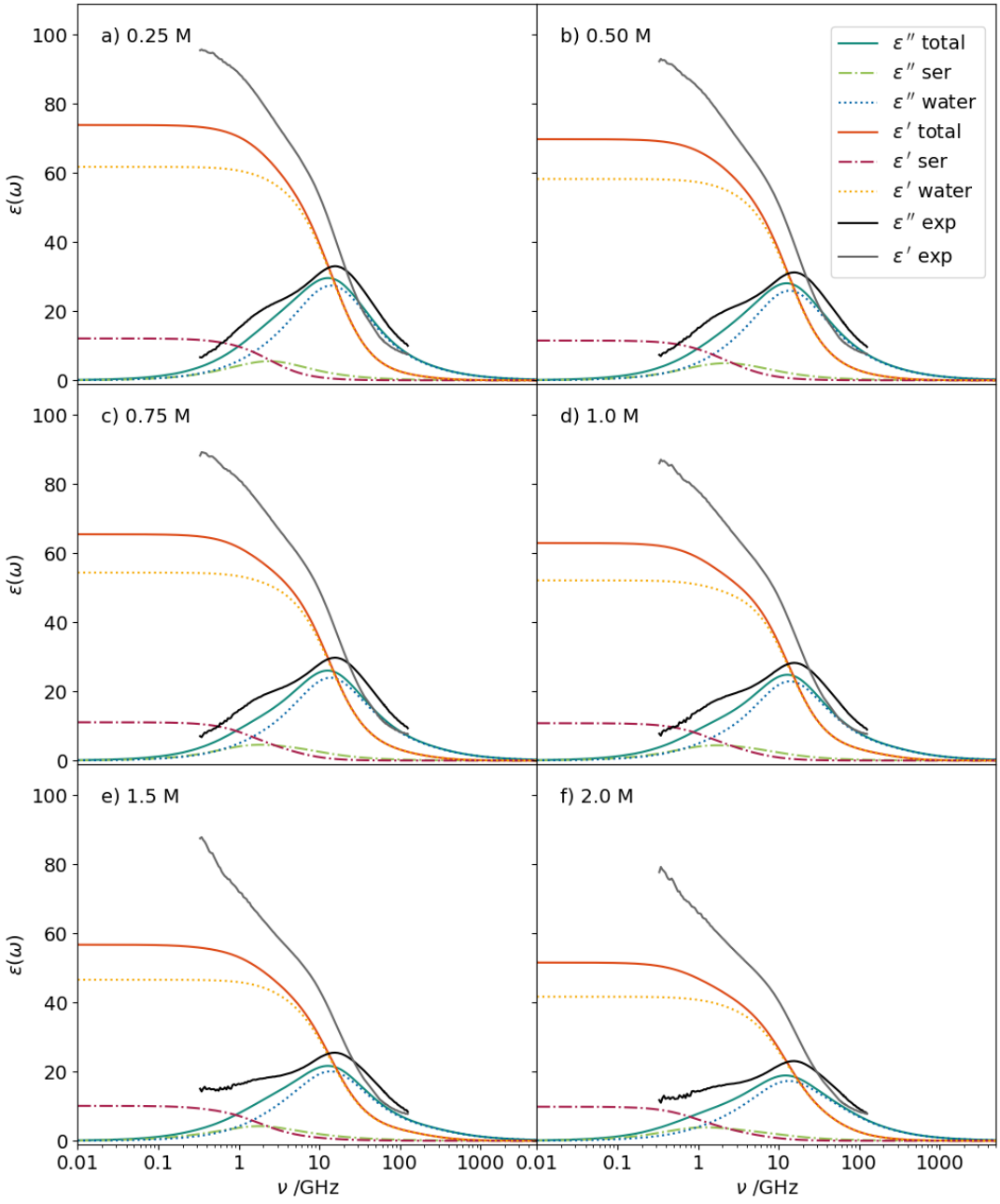

Figure 4.18: Dielectric spectra of serine and LiCl with a concentration of a) 0.25 M, b) 0.50 M, c) 0.75 M, d) 1.0 M, e) 1.5 M, f) 2.0 M in SPCE water.

Sodium chloride

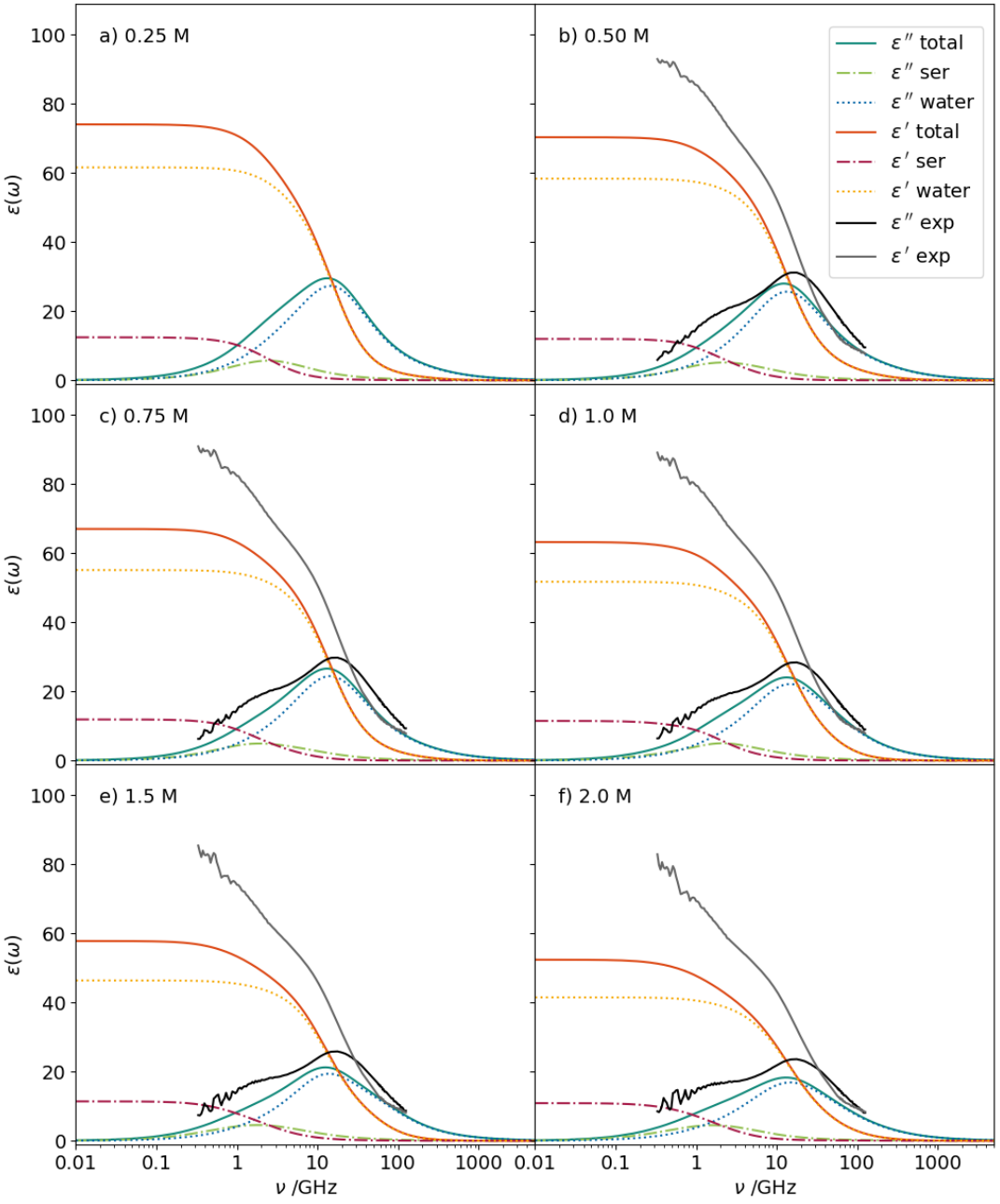

Figure 4.19: Dielectric spectra of serine and NaCl with a concentration of a) 0.25 M, b) 0.50 M, c) 0.75 M, d) 1.0 M, e) 1.5 M, f) 2.0 M in SPCE water.

4.2.4 Trends

The trends for the relative dielectric permittivity (ε_r) and dielectric relaxation times (τ) of the amino acids and water of arginine, lysine and serine systems are depicted in figure 4.20, 4.21 and 4.22, respectively. The trends from the MD simulations are depicted with points and solid lines, the ones from experimental data with diamonds and dash-dotted lines. The trends for potassium bromide, chloride and iodide are depicted in yellow, red and orange, respectively. The trends of systems containing lithium and sodium chloride are depicted in green and blue, respectively. The trends for potassium bromide are only plotted for spectra from MD simulations. There were little differences between potassium salts, therefore the experimental measurements were only repeated for potassium chloride and iodide in the second experiment. As the trends of the first experiment and the second experiment tend to differ significantly, the experimental data of potassium bromide from experiments were omitted in the plots. The plots only show mean values however, the data of computed spectra and experimental spectra have a high standard deviation.

The trends of the dielectric permittivity and relaxation times of arginine and water in arginine systems show good agreement with the experiments. The relaxation times of SPCE water are higher than that of water experimentally, which has been reported previously [51, 52]. Lysine systems also show good overall agreement with experimental data. The relaxation times of lysine and water are overestimated in simulations, but the trends follow the same magnitude. As discussed before, the dielectric permittivity and relaxation times of serine are lower in the computed spectra than in the experimental spectra. Even though the permittivity of the experiments is more than twice as high, the trends still show similar results. Therefore, even though the exact extent is not represented correctly, the ion specific effect on these properties are reproducible with MD simulations.

Considering specific ion effects, the cation seems to have a stronger effect on the dielectric decrement of the amino acids than the anion. In all cases the slope of the dielectric decrement of lithium chloride is the highest, followed by sodium chloride and potassium chloride. Therefore the order of cations influencing the dielectric decrement is:

$$K^+ < Na^+ < Li^+$$

With potassium leading to the least dielectric decrement, followed by sodium and lithium.

The effect of the anion on the dielectric decrement of the amino acids are not as conclusive. In computed serine mixtures, potassium chloride seems to decrease the permittivity the least, followed by potassium bromide and iodide. Experimental data shows the opposite trend for potassium chloride and iodide. The values from the computed spectra of serine and lysine scatter a lot which is why an exact order can not be made out. Overall, the dielectric decrement seems to be very similar for all potassium salts. The experimental data also only shows small differences between potassium iodide and chloride influencing the dielectric decrement of the amino acids.

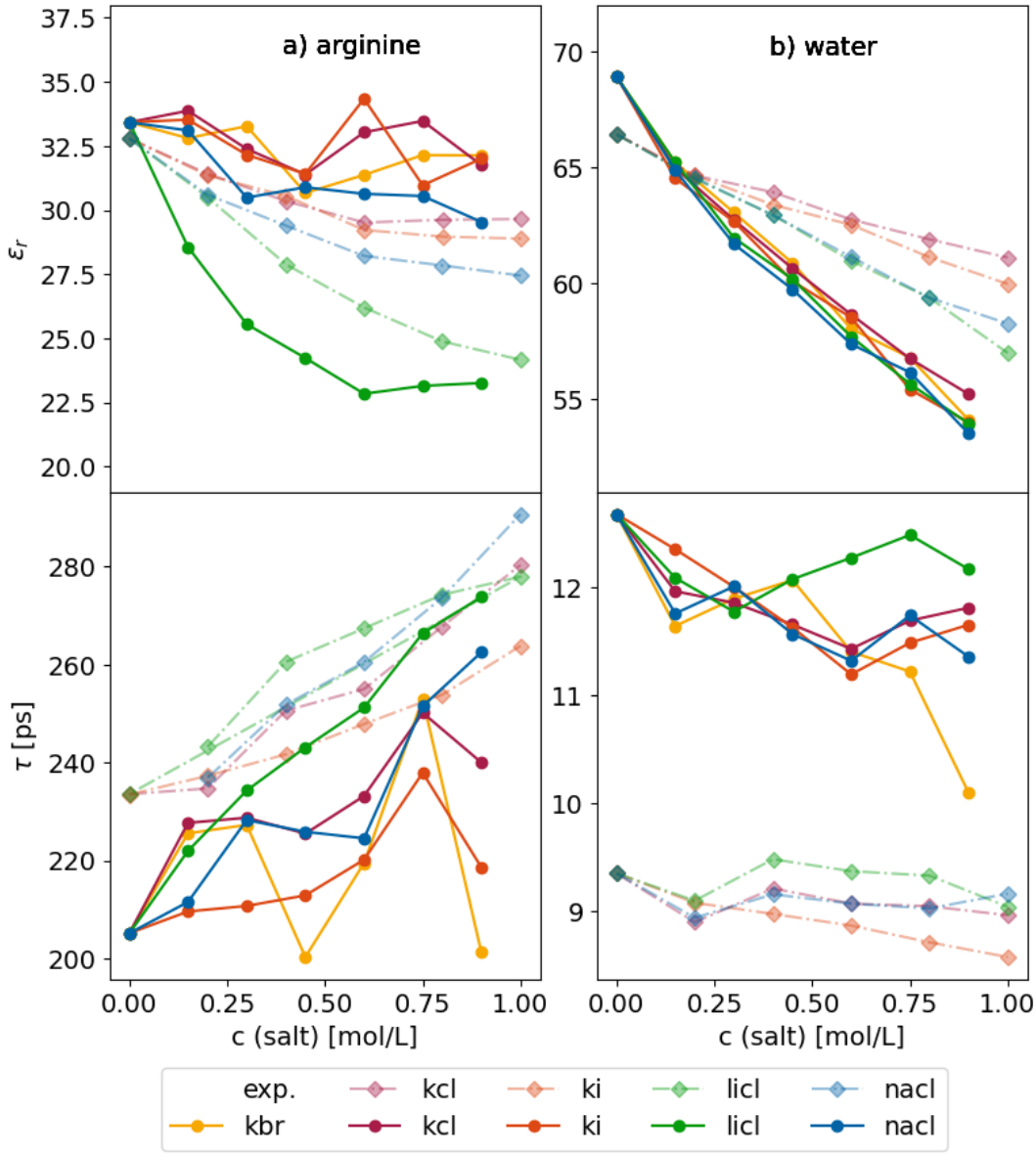

Figure 4.20: Dielectric permittivity (ε_r) and relaxation times (τ) of a) arginine and b) water. The diamonds and dash-dotted lines are experimental values, points and solid lines are calculated from the average of five replica of computed spectra.

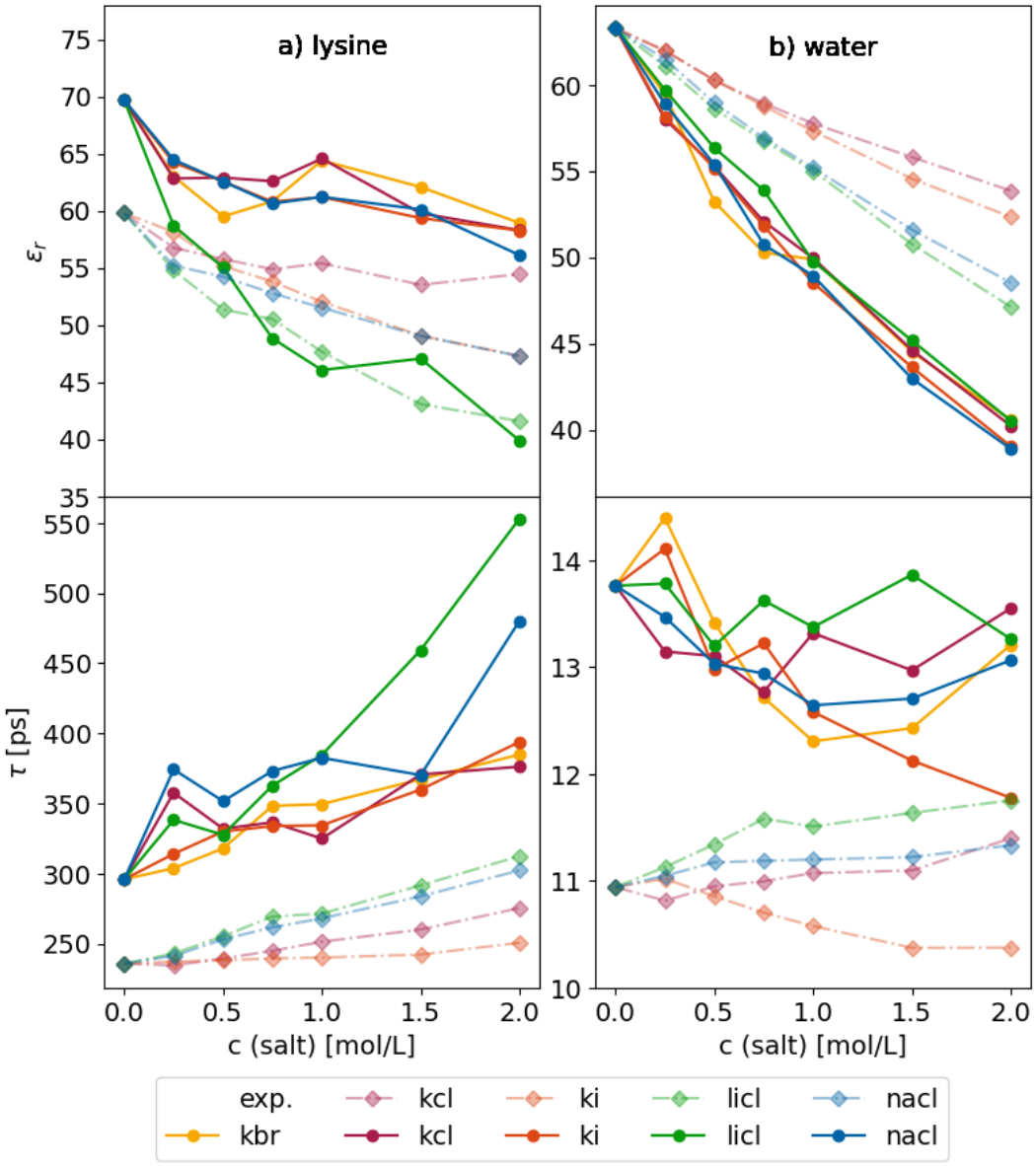

Figure 4.21: Dielectric permittivity (ε_r) and relaxation times (τ) of a) lysine and b) water. The diamonds and dash-dotted lines are experimental values, points and solid lines are calculated from the average of five replica of computed spectra.

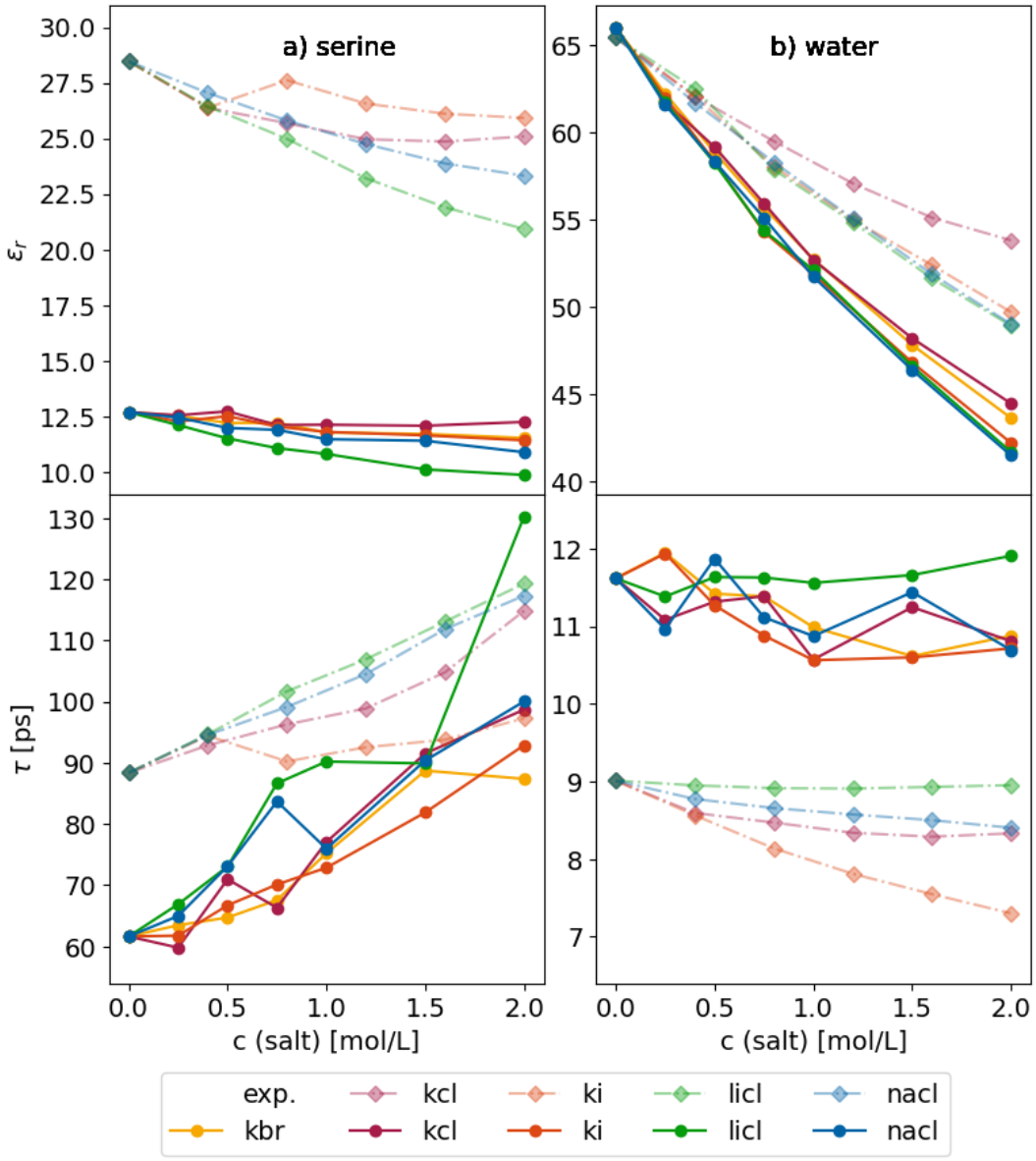

Figure 4.22: Dielectric permittivity (ε_r) and relaxation times (τ) of a) serine and b) water. The diamonds and dash-dotted lines are experimental values, points and solid lines are calculated from the average of five replica of computed spectra.

Different salts also influence the dielectric relaxation times of the amino acids. Here, the specific ion effects are similar to the trends of the permittivity in the case of amino acids, with cations seemingly having a bigger impact than anions. The relaxation times scatter more than the permittivity which is why an exact evaluation is not possible. However, some qualitative trends can still be made out. The steepest slope and therefore biggest change in relaxation times of the amino acid in all cases is due to lithium chloride. In the case of arginine and lysine the second steepest slope is that of sodium chloride systems. In the case of serine, the slope of sodium systems is about as high as the potassium salt systems. This could be caused by an outlier at 0.75 M skewing the slope. Potassium salts all have a relatively flat increment which makes them prone to errors. Overall, there seems to be a specific ion effect in cations concerning the relaxation times of the amino acids that is:

$$K^+ < Na^+ < Li^+$$

The anions do not show a reliable difference in trends of relaxation times of amino acids.

The relaxation times of water also change with increasing salt concentrations. In contrast to the relaxation times of amino acids, the anion seems to play a more important role. One notable property is that lithium chloride seems to have the least impact on relaxation times of water. The exact reason for this is unclear however, it could be due to less water molecules being necessary to solvatize lithium ions, or due to lithium being stronger coordinated to the amino acid which leaves more water molecules move unimpaired or a combination of both. Potassium bromide and iodide seem to have the highest impact on the relaxation time of water. More water molecules are needed to solvatize these ions because they are bigger. Additionally, there are less water molecules in total due to the size of the ions being bigger, meaning even a higher share of water molecules are in the solvation shell, compared to salts with smaller ions, as lithium or sodium and chloride. This can also be seen in the numbers of molecules packed in table 3.1, 3.2 and 3.3 for arginine, lysine and serine simulation boxes, respectively. Previous investigations on interactions of ionic liquids and proteins in aqueous solutions [53] showed that the anion of ionic liquids show stronger interactions with water, while the cation is pushed against the surface of the protein.

4.3 Radial distribution functions

4.3.1 Cation-oxygen

The interaction of the carboxylate group with the cation plays an important role considering specific ion effects [21]. Therefore, radial distribution functions were calculated for the carboxylate oxygen and the cation as well as the hydrogen oxygen and the cation. The RDF of oxygen and cations were calculated from the atom center. The g_{000} functions of oxygen and cations of arginine, lysine and serine systems are depicted in figure 4.23, 4.24 and 4.25, respectively. Overall the g_{000} decreases with increasing salt concentration. The

only exception for this phenomenon is lysine and sodium chloride systems. The RDF of the cation and oxygen seems to depend slightly on the anion. Looking at the potassium systems, one can see that the differences with increasing concentrations are highest with potassium chloride, followed by bromide and iodide for all amino acids. The size of the cation has a huge impact on the RDF. The smaller the cation, the lower the radius of the peak maximum. Potassium shows a peak maximum at radii just under 3 Å, sodium at about 2.5 Åand lithium at 2 Å. The maximal peak height is also strongly dependent on the cation. Lithium-carboxylate oxygen RDFs exhibit very high peaks with maxima of about 350, 185 and 85 in arginine, lysine and serine systems, respectively. Sodium-carboxylate oxygen RDFs have peak maxima of 40, 18 and 15 in arginine, lysine and serine systems, respectively. The g_{000} functions of the carboxylate group also exceeds the ones of oxygen of water and lithium or sodium. In the case of potassium the difference between cation-water oxygen RDFs and cation-carboxylate oxygen RDFs is not as pronounced.

Looking at the charges in table 3.4 of the carboxylate oxygen of the respective amino acid explains variations in the RDFs. The oxygen of arginine has the highest negative charge, followed by lysine and serine. Compared to these charges, the charge of oxygen in SPCE water is -0.8476 e. The charge of the oxygen of the carboxylate has a huge impact, which can be seen in the differences between the RDFs of the cation-carboxylate oxygen in systems with different amino acids with the same cation. Arginine has very high g_{000} values, especially for lithium and sodium and has a higher charge than water oxygen. The carboxylate oxygen of lysine has a slightly lower charge than the oxygen of water. Yet, the g_{000} values of lithium and sodium exceed those of water, whereas those of potassium are similar. This is probably due to the size of the ions. The same effect is visible in serine systems, even though serine has an even lower charge than lysine. However, due to the carboxylate group having two charged oxygen close to each other the net attraction to the cation can still be higher than in water. Additionally there are differences in σ and ϵ, which are 0.3166 nm and 0.650 eV for oxygen in water and 0.296 nm and 0.879 eV for carboxylate oxygen.

4.3.2 Binary mixtures

The RDF of the amino acid water mixtures are calculated from the center of mass and are depicted in figure 4.26. The g_{000} is the solid line, g_{110} is the dash-dotted line. The RDF of water-water pair distributions are blue, amino acid-amino acid pair distributions are red and amino acid-water pair distributions are orange.

Looking at amino acid-amino acid interactions, all amino acids show a minimum at approximately 5 Å in the g_{110} function, which corresponds to two amino acid molecules in a stacked position like in figure 4.27 a) and e). The g_{000} function at 5 Å shows a local maximum in the case of arginine. This means the stacked position is slightly more favored than positions close to it even though at this distance arginine is still depleted from other arginine molecules, as the function is below one. In the case of lysine, the stacked position is depleted in concentration compared to their global concentration. In the case of serine, the g_{000} rises above one before minimum in the g_{110} function meaning the stacked position is preferred.

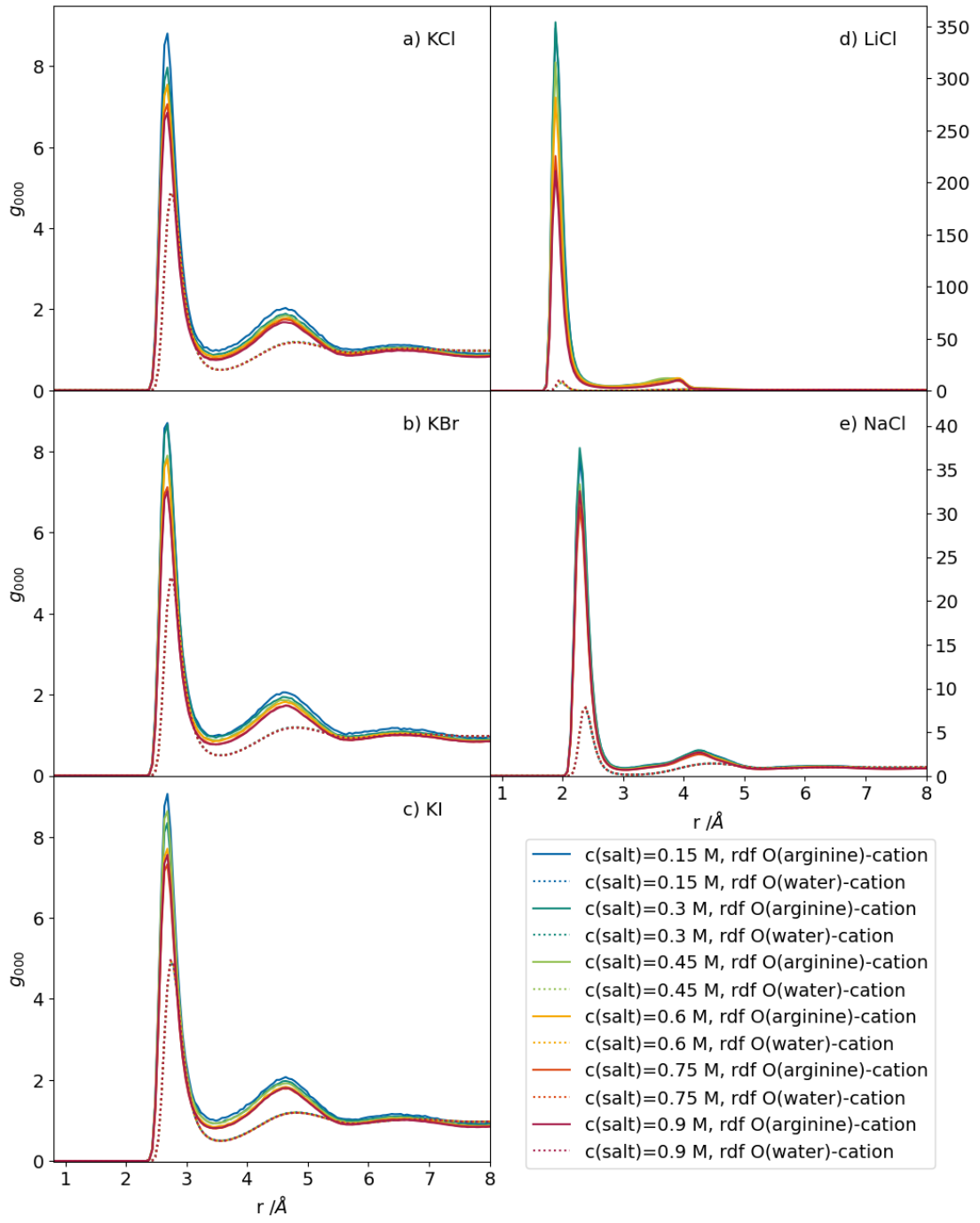

Figure 4.23: Radial distribution function of the respective cation and oxygen from the carboxylate group of the amino acid (solid line) and water (dotted lines) of arginine systems.

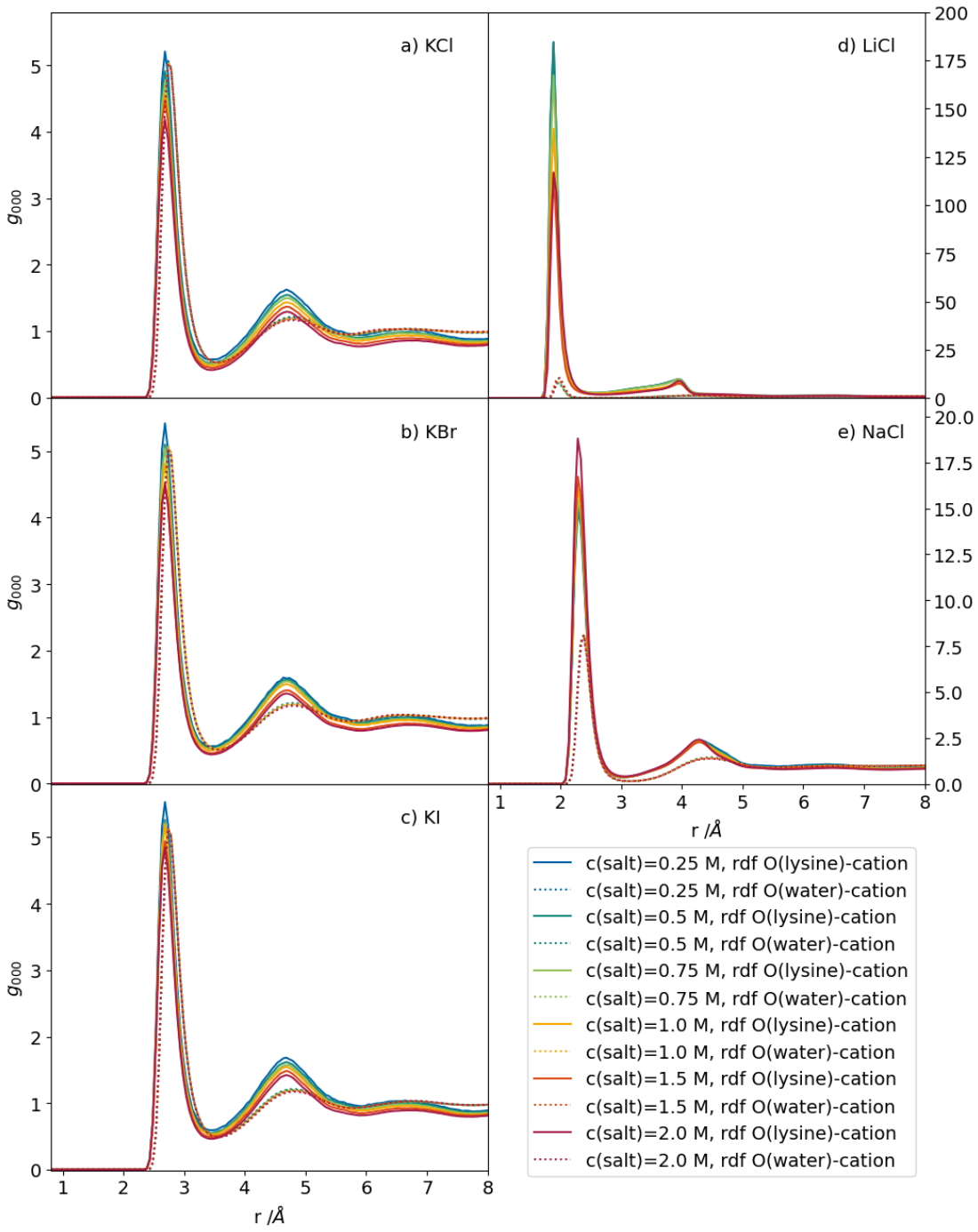

Figure 4.24: Radial distribution function of the respective cation and oxygen from the carboxylate group of the amino acid (solid line) and water (dotted lines) of lysine systems.

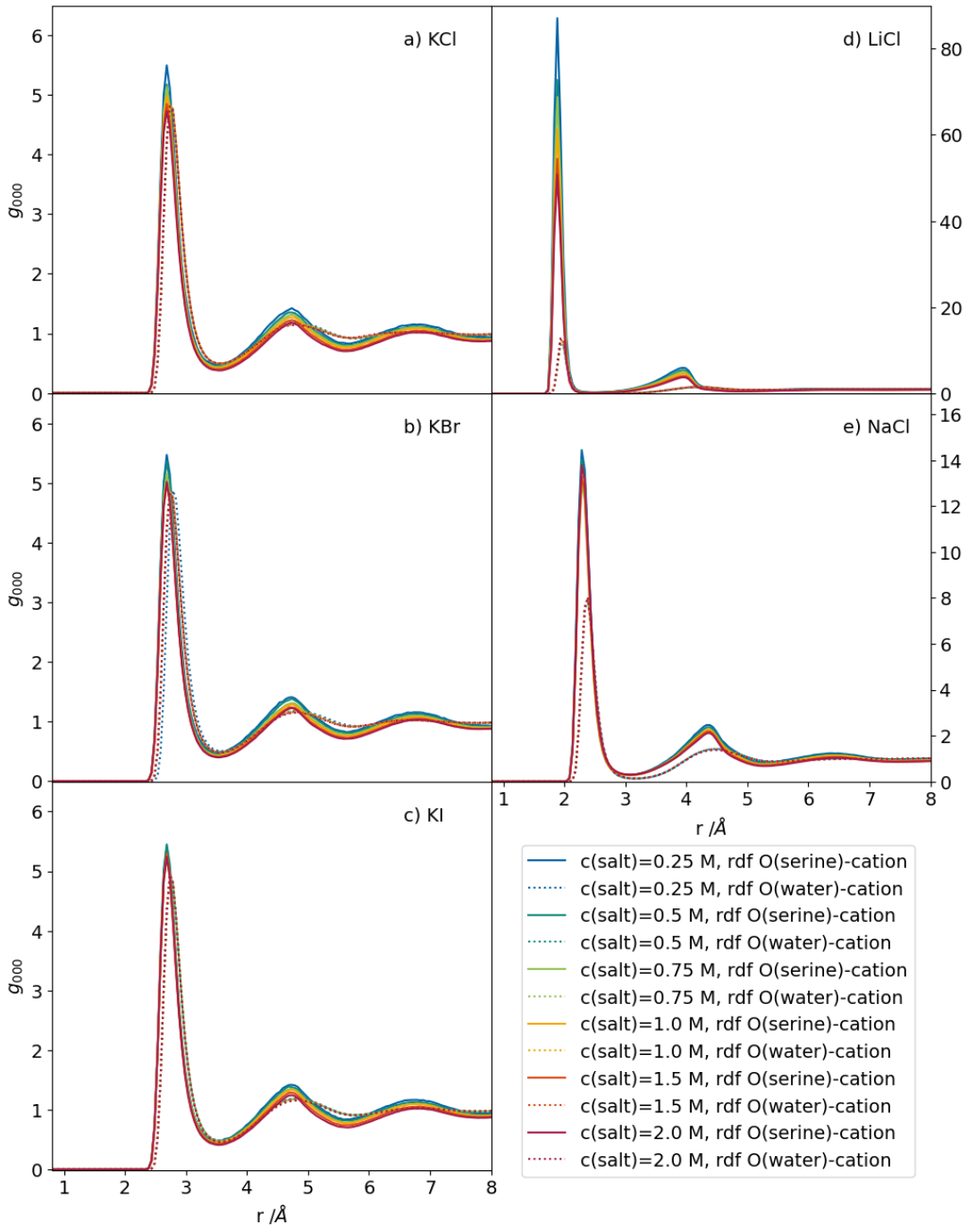

Figure 4.25: Radial distribution function of the respective cation and oxygen from the carboxylate group of the amino acid (solid line) and water (dotted lines) of serine systems.

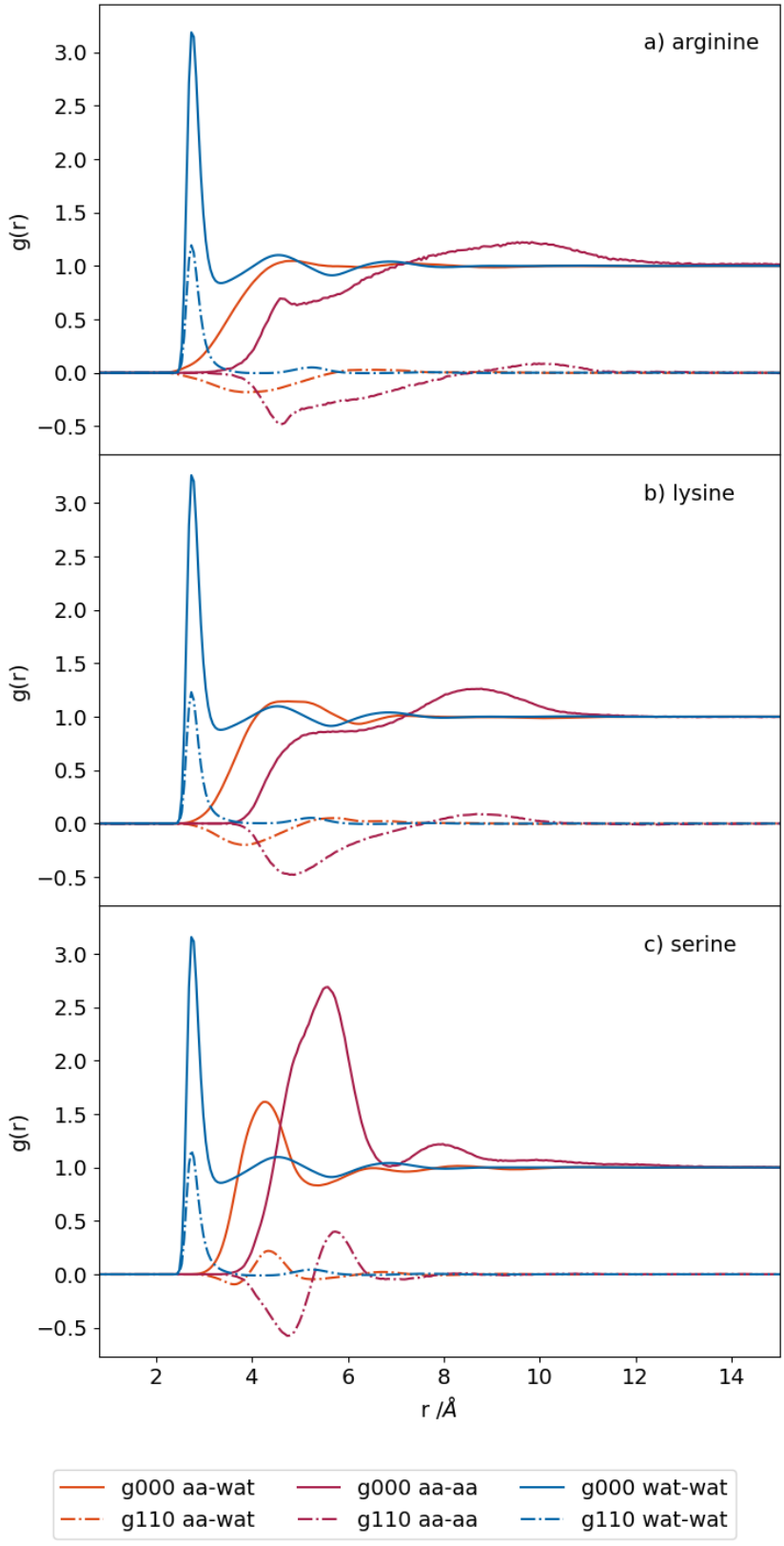

 Figure 4.26: RDF of the three amino acids, a) arginine, b) lysine, and c) serine.

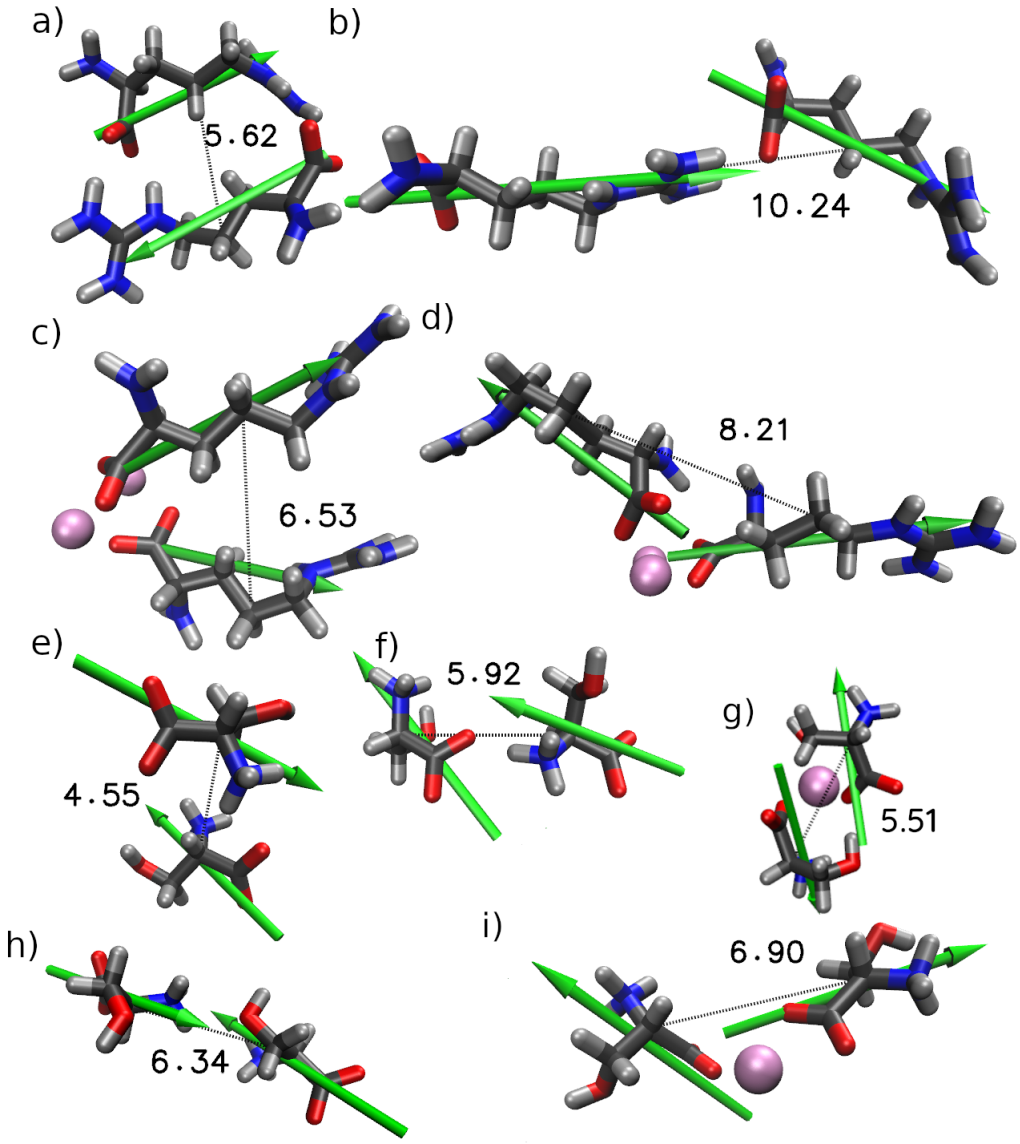

Figure 4.27: Example snap shots of two amino acid molecules aligned in a stacked position in a), c), e) and g) and in a chain like position in b), d), f), i) and h). a), b), e), f) and h) shows snap shots from simulations without added salts, c), d), g) and i) show examples from simulations with LiCl. Here the Li^+ ion acts as a coordinator. Pictures a)-d) show arginine and e)-i) show serine.

The positive peak in the g_{110} function of amino acid-amino acid pair distributions is at approximately 10 Å in the case of arginine, 8.5 Å in the case of lysine and 6 Å in the case of serine. This maximum origins from amino acids forming chain like structures from their partial positive side chains in the case of arginine and lysine and the α-amino group of serine to the negative carboxylate end, as shown in figure 4.27 b) and f). The g_{000} function also shows a maximum at this distance, meaning that chain like positions are favored by all amino acids. Serine shows a local minimum right after at around 7 Å in both g-functions. This is due to it forming chain like structures with anti-parallel dipole alignment from the α-amino group to the side chain alcohol group like in figure 4.27 h).

The g_{000} function of water-water pair interactions are quasi independent from the amino acid due to water being the solvent and therefore present in excess. Concentrations of amino acids in this range do not have a big impact on the distances for minima and maxima compared to pure water. The first maximum of the g_{000} function is at 2.74 Å, the second maximum is at 4.54 Å, the third maximum is at 6.89 Å. Comparing the values of computational data [54] for SPCE water, the first, second and third peak is at 2.75 Å, 4.50 Å and 6.83 Å, respectively which shows good agreement with the computational data. Data for the g_{110} functions for water can be found in reference [55] and are also similar to the results from binary mixtures, which show a high maximum at low distances, and are only slightly negative in the following minimum.

Amino acid-water pair interactions seem to be comparably weak. The g_{000} function has a maximum at nearly the same distance as the stacked position of the amino acid-amino acid. This corresponds to the first solvation shell. The peak is broadened due to anisotropy of the amino acids, which is clearly visible in the lysine spectrum. The g_{110} function is negative at this point in the case of arginine and lysine, meaning the dipole moment of water and arginine are in slightly opposing directions. In the case of serine, the amino acid-water g_{110} function starts off negative but has a maximum where the g_{000} function has a maximum.

4.3.3 Salt mixtures

The g_{000} radial distribution functions and g_{110} dipole-dipole spatial correlation functions functions are depicted in figure 4.28, 4.29 and 4.30 for arginine, lysine and serine systems, respectively. Potassium salts seem to have little effect on the amino acid-amino acid pair distribution.

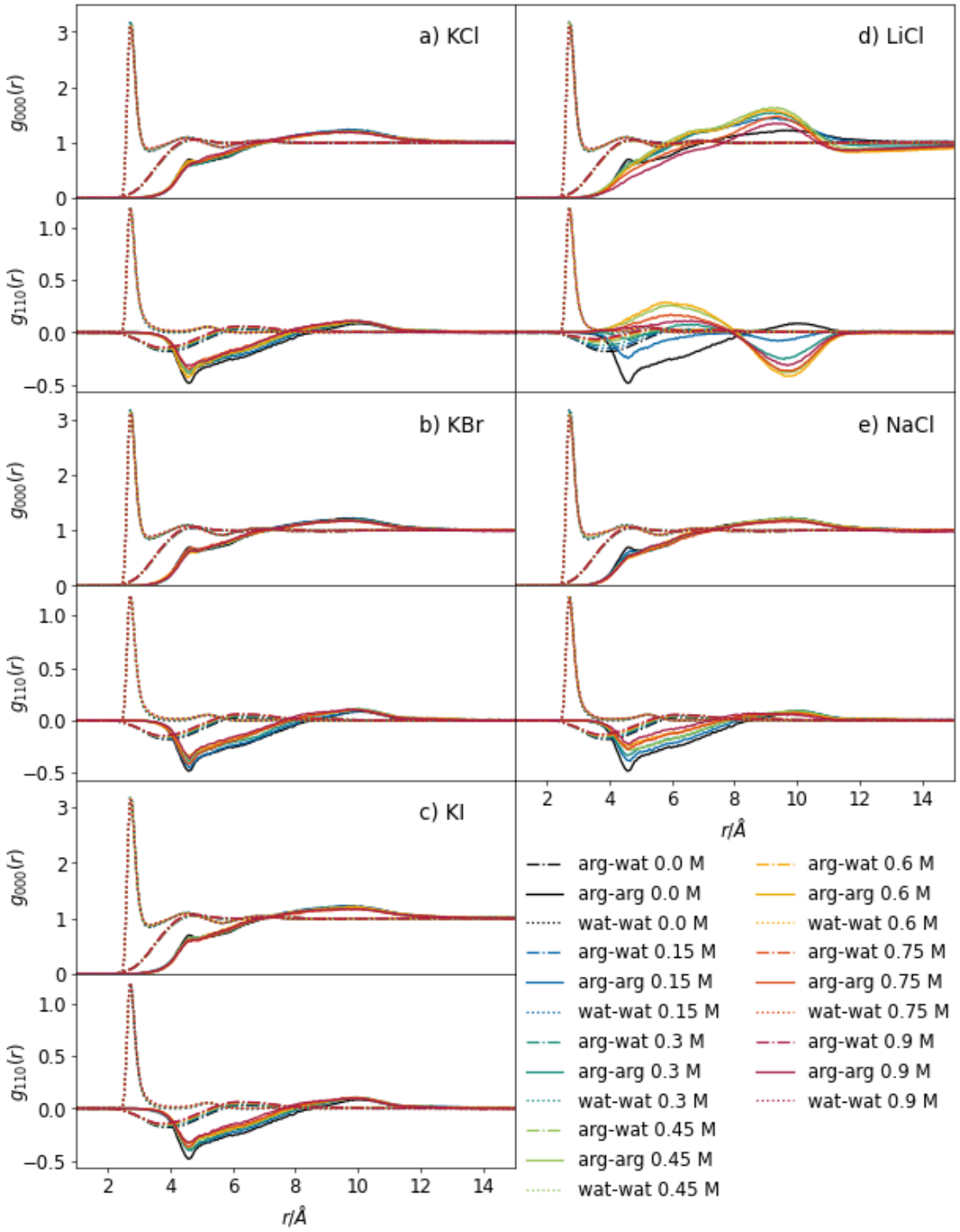

Figure 4.28: Radial distribution functions $g_{000}$and g_{110} of arginine.

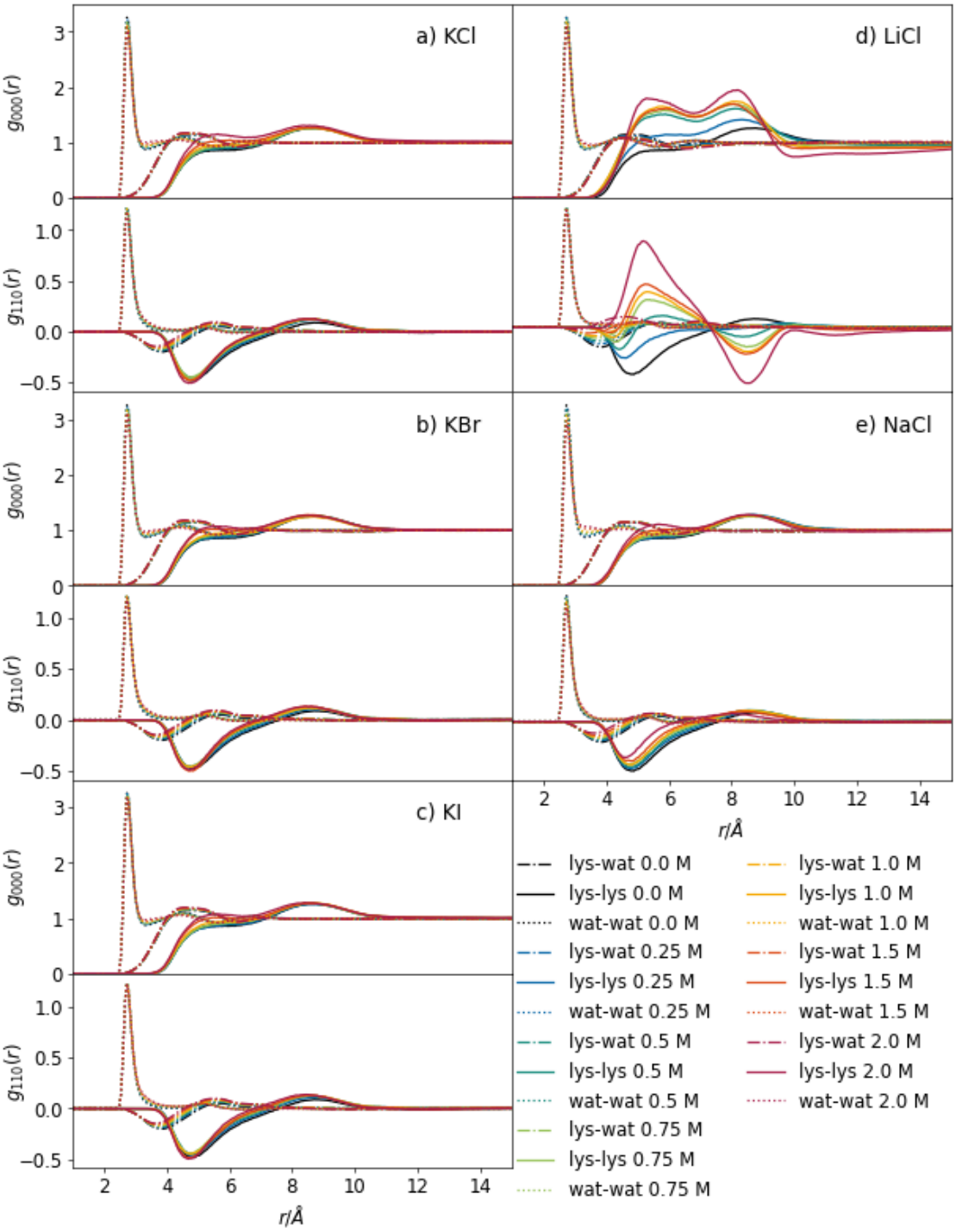

Figure 4.29: Radial distribution functions $g_{000}$and g_{110} of lysine.

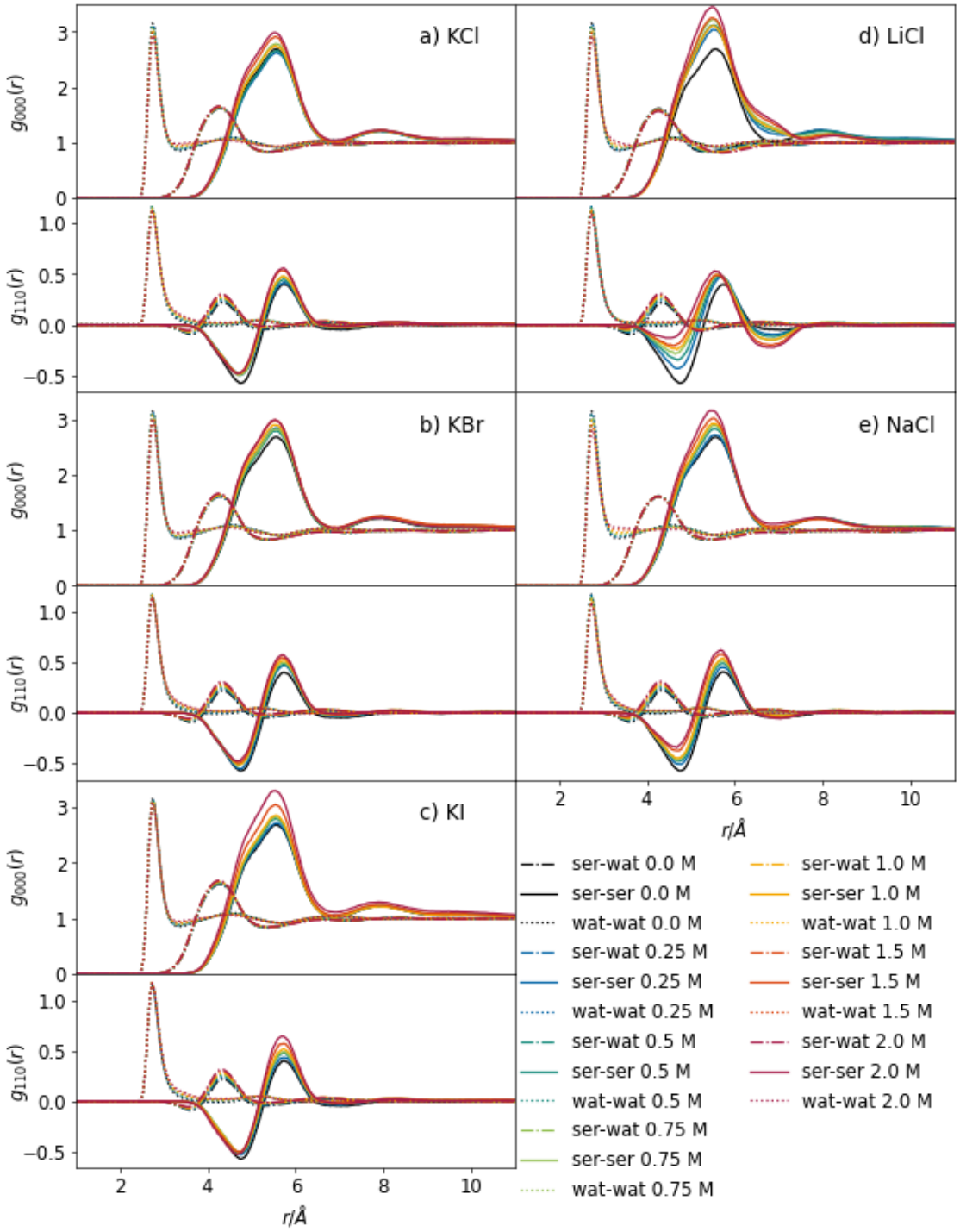

Figure 4.30: Radial distribution functions g_{000} and g_{110} of serine.

Table 4.1: Values of the stacked and chain like position (based on minima and maxima of the g_{110} function) for the amino acid-amino acid 0.45 M arginine, 1.0 M lysine and serine with 0.90 M (arginine) and 2.0 M (lysine/serine) solutions of the respective salts.

		stacked			chain		
Amino acid	Salt	r Å	g_{000}	g_{110}	r Å	g_{000}	g_{110}
Arginine	KBr	4.64	0.643	-0.367	9.89	1.167	0.106
	KCl	4.54	0.561	-0.317	9.84	1.18	0.110
	KI	4.59	0.588	-0.333	9.49	1.17	0.0966
	LiCl	6.39	0.806	0.110	9.69	1.32	-0.316
	NaCl	4.64	0.588	-0.230	8.44	1.13	0.0668
	no salt	4.59	0.695	-0.483	9.99	1.21	0.0858
Lysine	KBr	4.74	0.870	-0.493	8.44	1.27	0.133
	KCl	4.69	0.884	-0.507	8.49	1.30	0.128
	KI	4.69	0.842	-0.494	8.44	1.28	0.137
	LiCl	5.14	1.50	0.877	8.59	1.76	-0.569
	NaCl	4.63	0.937	-0.348	8.04	1.24	0.0771
	no salt	4.89	0.774	-0.480	8.84	1.26	0.0889
Serine	KBr	4.69	1.88	-0.475	5.74	2.82	0.571
	KCl	4.69	1.88	-0.482	5.69	2.87	0.553
	KI	4.69	2.06	-0.529	5.74	3.11	0.643
	LiCl	4.54	3.43	-0.129	5.59	3.39	0.527
	LiCl	(third exteme)			6.74	1.46	-0.222
	NaCl	4.69	1.93	-0.345	5.64	3.05	0.606
	no salt	4.74	1.75	-0.576	5.69	2.63	0.395

Arginine
Stacked:
g_{000}, all are depleted (<1)

$$\text{KCl (most depleted)} < \text{NaCl} = \text{KI} < \text{KBr} < \text{no salt} < \text{LiCl (least depleted)}$$

g_{110}

$$\text{no salt (most negative)} < \text{KBr} < \text{KI} < \text{KCl} < \text{NaCl (least negative)} < \text{LiCl (positive)}$$

Potassium bromide, chloride, iodide and sodium chloride systems have less molecules in stacked position compared to when no salt is added. The dipole moments align less anti-parallel in total than in solutions with no salt added. Less molecules in less anti-parallel orientation lead to enhancement of permittivity compared to no salt. Lithium chloride systems have more molecules in stacked position but the stacked position is parallel and therefore the permittivity is enhanced compared to when no salt is added.
Chain:
g_{000}, all are enriched (>1)

$$\text{NaCl (least enriched)} < \text{KBr} < \text{KI} < \text{KCl} < \text{no salt} < \text{LiCl (most enriched)}$$

g_{110}

$$\text{LiCl (negative)} < \text{NaCl (least positive)} < \text{no salt} < \text{KI} < \text{KBr} < \text{KCl (most positive)}$$

Potassium salts change the alignment so that the arginine molecules' dipole moment is more parallel than when no salt is added, which would increase the permittivity but there are less molecules in this positions. This means there is a competing process. Overall, the permittivity decreases in the dielectric spectra. Sodium chloride leads to dipole moments of arginine being less parallel and there are less molecules in this positions, both factors decrease the permittivity. Lithium chloride causes more molecules to be in the chain like position compared to when no salt is added, but their dipole moment aligns anti-parallel. This leads to a decrease in permittivity.

Comparing the stacked and chain like formation from KBr, KCl, and KI, arginine gains permittivity from the stacked position as the orientation is slightly less anti-parallel and there are less molecules in this position. In the chair like position are competing factors. One the one hand the dipole moment is aligned more parallel than when no salt is added, but on the other hand there are less molecules in that position. Overall, the permittivity increases with increasing salt concentrations, which would imply that factors that decrease permittivity outplay factors that increase permittivity.

Arginine in sodium chloride mixtures gains permittivity from the stacked position as there are less molecules in that position and the total dipole moment alignment is less anti-parallel. In the chain like position however, the permittivity decreases as there are less molecules in that position and the total dipole moment is less parallel aligned. These are competing factors. Similar to potassium salts, the permittivity decreases which would imply the factors leading to decreased permittivity are stronger.

In the case of lithium chloride solutions both, the chain like formation and the stacked position are highly populated compared to when no salt is added. The stacked position however, is still depleted compared to the global concentration and the chain like formation is enriched. The stacked position has parallel alignment of the dipole moment of arginine whereas the chain like formation has anti-parallel alignment of the dipole moment. As the chain like formation is favored the permittivity decreases overall.

Lysine

Stacked:

g_{000}

$$\text{no salt (most depleted)} < \text{KI} < \text{KBr} < \text{KCl} < \text{NaCl (least depleted)} < \text{LiCl (enriched)}$$

g_{110}

$$\text{KCl (most negative)} < \text{KI} < \text{KBr} < \text{no salt} < \text{NaCl (least negative)} < \text{LiCl (positive)}$$

There are more lysine molecules in the stacked position when potassium salts are added compared to when no salt is added and their dipole moment is aligned more anti-parallel. This leads to a decreased permittivity. In sodium chloride solutions, the maximum of the g_{000} function is slightly shifted from the minimum of the g_{110} function with increasing salt concentration. The radius at the minimum value of the g_{110} has a corresponding value of the g_{000} function of slightly below one, which would mean it is depleted. However, at higher radii, the g_{110} is still negative and the g_{000} is positive, which means similar positions to perfectly stacked molecules are even preferred. The g_{110} function is less negative with increasing salt concentration. Those are competing factors. One one hand there are more lysine molecules in an anti-parallel position which would decrease the permittivity. However, the g_{110} is less negative which increases the permittivity. Lithium chloride leads to more lysine molecules in the stacked position compared to when no salt is added and their dipole moment is parallel. Both factors increase the permittivity.

Chain:

g_{000}, all are enriched (>1)

$$\text{NaCl (least enriched)} < \text{no salt} < \text{KBr} < \text{KI} < \text{KCl} < \text{LiCl (most enriched)}$$

g_{110}

$$\text{LiCl (negative)} < \text{NaCl (least positive)} < \text{no salt} < \text{KI} < \text{KBr} < \text{KCl (most positive)}$$

Adding potassium salts leads to slightly more lysine molecules in the chain like position and their dipole moment is more aligned, which increases permittivity. Sodium chloride causes less arginine molecules to be in this position and their dipole moments are less aligned, which both decreases the permittivity. Lysine in solutions with lithium chloride align more in a chain like position compared to when no salt is added but their dipole moments are anti-parallel. This decreases the permittivity. In the case of the all salts there are competing factors changing the permittivity that have to be taken into account.

Serine

Stacked:

g_{000}, all enriched > 1

no salt (least enriched) < KBr < KCl < NaCl < KI < LiCl (most enriched)

g_{110}

no salt (most negative) < KI < KCl < KBr < NaCl < LiCl(least negative)

For all potassium salts and sodium chloride solutions, the stacked position of serine, shown in figure 4.27 e) is more enriched compared to when no salt is added. This would lead to a decrease of the permittivity. However, g_{110} shows that the stacked position is also less anti-parallel aligned which would increase the permittivity. Lithium chloride causes more serine molecules to be in a stacked position and their dipole moment is overall anti-parallel aligned but less anti-parallel than when no salt is added. In the case of serine there are two possibilities for two serine molecules to be coordinated by lithium in a stacked position. One has parallel aligned dipole moments and looks similar to arginine in figure 4.27 c), one has anti-parallel aligned dipole moments, visualized in figure 4.27 g). Additionally, even with lithium in solution there is still the anti-parallel aligned stacked position present that has no lithium coordinated.
Chain:
g_{000}, all are enriched (>1)

no salt (least enriched) < KBr < KCl < NaCl < KI < LiCl (most enriched)

g_{110}

no salt (least positive)< KCl < KBr < NaCl < KI (most positive)

There are more serine molecules in the chain formation when potassium salts or sodium chloride is added compared to when no salt is added. This leads to an increase of the permittivity. However, their dipole moment is less aligned which decreases the permittivity. These are competing factors. Adding lithium chloride leads to more molecules in a chain like position compared to when no salt is added but they are less parallel aligned. These are competing factors. Lithium leads to a second chain like formation, which is the anti-parallel aligned position with a radius of about 6.735 Å. This formation decreases the permittivity.

Lithium leads to coordination of all amino acids. This is due to the lithium ions high affinity to the carboxylate which makes lithium acting as a link between two carboxylate ions reversing the alignment of the dipole moments in stacked and chain like structures. In figure 4.27 c) one can see that the stacked arginine molecule's dipole moments are aligned due to them both being coordinated to the lithium ion. Coordination happens in chain like formation too, depicted in figure 4.27 d) and i) resulting in anti-parallel alignment of the amino acid's dipole moments. The lithium ion act as a a strong coordinator between the two carboxylate groups which would repel each other without it. In arginine and lysine systems, it can be seen in the g_{110} of the amino acids. With increasing lithium chloride concentration, the minimum at 5 Å becomes a maximum and the following maximum becomes a minimum even at concentrations as low as 0.15 M-0.3 M and 0.5 M in arginine and lysine solutions, respectively. Serine also shows the strongest change in the g-functions

with lithium ions being present. The stacked position at approximately 5 Å becomes less anti-parallel aligned and the parallel coordinated chain like position at 7 Å becomes more anti-parallel and more populated with increasing lithium ion concentration. The chain like formation at 6 Å is more affected than in solutions with other salts. However, there is no reversal in the alignment of the dipole moments in lithium chloride and serine solutions as it is in the case of lysine and arginine. The reason for serine being less influenced by lithium than the other amino acids could be due to the partial charges on the carboxylate group. The partial charges on the oxygen atoms of the carboxylate group of serine are lower than those of the oxygen atoms in water, whereas in the case of arginine and lysine they are higher. For lithium the dielectric decrement seems to stem through coordination of ions, similar to the dielectric decrement that happens in water through hydration of ions.

Comparing the g_{000} to the g_{110} functions for water-water pair interactions, one can see that the presence of salts has also influence on the g_{110} function. This effect arises from the rearrangement of dipole orientations within the solvation shells of he cation and the anion [55]. One can observe that effect on all amino acids. The initial peak at 2.735 Å decreases with increasing salt concentration in the g_{000} as well as the g_{110}. Comparing the maximal values of the first peak, listed in table 4.2, the order of deviance of the maximal peak height without salt is:

$$\mathrm{KI} < \mathrm{KBr} < \mathrm{KCl} < \mathrm{NaCl}$$

with Lithium being in the range before KCl to after KBr depending on the g-function and amino acid. The reason LiCl is less disturbing to the water structure than the Hofmeister series would suggest is due to the strong coordination to the amino acid. When lithium is coordinated to the amino acid, less water ions are needed to solvatize lithium ions. Looking at the g_{000}, the peak height of the lysine-KBr system is slightly higher than the LiCl system. However, when looking at the g_{110} the maximum of the lysine-LiCl system is higher than that of KBr. Arginine shows similar results considering the sequence but LiCl is about as disruptive as KCl. In the case of serine LiCl is the second most perturbing salt. The extent of disorder LiCl has on water is strongly affected by the amino acid, due to lithium coordinating to the amino acid. Overall, the series from chaotropic to kosmotropic of the cations is close to the Hofmeister series, with the exception of sodium and lithium being switched. The anions show typical behavior regarding the hydration. Iodide shows the weakest hydration and chloride the strongest. This leads to a reverse Hofmeister series regarding the disturbance of the water structure.

$$\mathrm{K^+} < \mathrm{Li^+} < \mathrm{Na^+}$$
$$\mathrm{I^-} < \mathrm{Br^-} < \mathrm{Cl^-}$$

Table 4.2: Values of g_{000} and g_{110} for the water-water interaction at the first peak maximum for 0.45 M arginine, 1.0 M lysine/serine with 0.90 M (arginine) and 2.0 M (lysine/serine) solutions of the respective salts.

Amino acid	Salt	g_{000} 1st peak	g_{110} 1st peak
Arginine	KBr	3.11	1.19
	KCl	3.08	1.18
	KI	3.15	1.21
	LiCl	3.10	1.18
	NaCl	3.04	1.15
	no salt	3.19	1.19
Lysine	KBr	3.08	1.18
	KCl	3.02	1.16
	KI	3.16	1.21
	LiCl	3.07	1.20
	NaCl	2.91	1.10
	no salt	3.26	1.23
Serine	KBr	2.98	1.14
	KCl	2.93	1.12
	KI	3.07	1.17
	LiCl	2.91	1.10
	NaCl	2.82	1.06
	no salt	3.16	1.16

5 Conclusions and outlook

Specific ion effects could be found for all three amino acids in solutions with different salts and concentrations influencing the behavior of the amino acids. The effects are visible in the dielectric spectra of amino acids in aqueous electrolyte solutions. The extent of the specific ion effects depend on concentration of the respective ions and the amino acid they interact with. The effect on dielectric parameters of amino acids seem to be stronger for monovalent cations than anions. Lithium has the strongest effect on dielectric permittivities and relaxation times of the investigated amino acids arginine, lysine and serine. The dielectric permittivity of the amino acid decreases with increasing salt concentrations in all cases, but the dielectric decrement is the highest with lithium chloride, considering the inspected salts potassium bromide, chloride and iodide as well as lithium and sodium chloride. The relaxation times of the amino acids are also strongly dependent on the salts and their concentration. Increasing the salt concentration lead to an increased relaxation time of the amino acid. This effect is also dominated by cations with lithium showing the strongest increase in relaxation times on all amino acids. The effect on the permittivity and relaxation times of the amino acids is second strongest in sodium chloride solutions. From the salts investigated, potassium salts have the least impact on the permittivity and relaxation times of the amino acids. Comparing computational and experimental data, potassium iodide leads to a higher dielectric decrement of the amino acids arginine and serine but has a smaller impact on their relaxation times than potassium chloride. The computed data shows a reversed effect on lysine, however the values of potassium iodide and chloride are close so that an exact statement cannot be made.

The dielectric permittivity and relaxation time of water is also sensitive to ion specific effects. Similar to the relaxation times of the amino acids water also shows a dielectric decrement. Lithium chloride leads to the highest decrement and potassium salts to the lowest, akin to the amino acids. The relaxation times of water however show the opposite effect with lithium having the smallest impact on the relaxation time of water.

Further studies regarding the orientation of amino acid molecules that are coordinated to each other will show if the hypotheses made from the radial distribution functions are correct. For this a Voronoi analysis combined with a dipole-dipole correlation function could be made to calculate orientations of neighboring molecules.

One interesting phenomenon that needs to be further investigated is why lithium does seemingly not affect the relaxation time of water. The differences between the relaxation times of water depending on the ions could be analyzed using Voronoi analysis. Studying the volumes of bulk and hydration water could give information on the mobility of the respective ions and therefore information on the water dynamic.

Bibliography

[1] F. Hofmeister, "Zur Lehre von der Wirkung der Salze: Zweite Mittheilung," 1888.

[2] K. P. Gregory et al., "Understanding specific ion effects and the hofmeister series," *Phys. Chem. Chem. Phys.*, vol. 24, pp. 12682–12718, 2022.

[3] R. Curtis and L. Lue, "A molecular approach to bioseparations: Protein–protein and protein–salt interactions," *Chemical Engineering Science*, vol. 61, no. 3, pp. 907–923, 2006. Biomolecular Engineering.

[4] A. S. Parmar and M. Muschol, "Hydration and hydrodynamic interactions of lysozyme: Effects of chaotropic versus kosmotropic ions," *Biophysical Journal*, vol. 97, no. 2, pp. 590–598, 2009.

[5] H. I. Okur, J. Hladílková, K. B. Rembert, Y. Cho, J. Heyda, J. Dzubiella, P. S. Cremer, and P. Jungwirth, "Beyond the hofmeister series: Ion-specific effects on proteins and their biological functions," *The Journal of Physical Chemistry B*, vol. 121, no. 9, pp. 1997–2014, 2017.

[6] J. B. Hasted, D. M. Ritson, and C. H. Collie, "Dielectric Properties of Aqueous Ionic Solutions. Parts I and II," *The Journal of Chemical Physics*, vol. 16, pp. 1–21, 1 1948.

[7] R. Buchner, G. T. Hefter, and P. M. May, "Dielectric relaxation of aqueous nacl solutions," *The Journal of Physical Chemistry A*, vol. 103, no. 1, pp. 1–9, 1999.

[8] W. Wachter, W. Kunz, R. Buchner, and G. Hefter, "Is there an anionic hofmeister effect on water dynamics? dielectric spectroscopy of aqueous solutions of nabr, nai, nano3, naclo4, and nascn," *The Journal of Physical Chemistry A*, vol. 109, no. 39, pp. 8675–8683, 2005.

[9] R. Buchner and G. Hefter, "Interactions and dynamics in electrolyte solutions by dielectric spectroscopy," *Phys. Chem. Chem. Phys.*, vol. 11, pp. 8984–8999, 2009.

[10] R. Gulich, M. Köhler, P. Lunkenheimer, and A. Loidl, "Dielectric spectroscopy on aqueous electrolytic solutions," *Radiation and Environmental Biophysics*, vol. 48, no. 1, pp. 107–114, 2009.

[11] B. Maribo-Mogensen, G. M. Kontogeorgis, and K. Thomsen, "Modeling of dielectric properties of aqueous salt solutions with an equation of state," *The Journal of Physical Chemistry B*, vol. 117, no. 36, pp. 10523–10533, 2013.

[12] N. Gavish and K. Promislow, "Dependence of the dielectric constant of electrolyte solutions on ionic concentration: A microfield approach," *Phys. Rev. E*, vol. 94, p. 012611, Jul 2016.

[13] J. C. W. Shepherd and E. H. Grant, "Dielectric properties of amino acid solutions. i. dielectric dispersion in aqueous ε-aminocaproic acid solutions," *Proceedings of the Royal Society of London. Series A, Mathematical and Physical Sciences*, vol. 307, no. 1490, pp. 335–344, 1968.

[14] U. Kaatze, H. Bieler, and R. Pottel, "Dielectric spectroscopy on aqueous solutions of some zwitterionic amino acids," *Journal of Molecular Liquids*, vol. 30, no. 2, pp. 101–113, 1985.

[15] T. Sato, R. Buchner, Šarka Fernandez, A. Chiba, and W. Kunz, "Dielectric relaxation spectroscopy of aqueous amino acid solutions: dynamics and interactions in aqueous glycine," *Journal of Molecular Liquids*, vol. 117, no. 1, pp. 93–98, 2005. Routes from Local Order to Large Scale Cooperativity.

[16] V. Raicu and Y. Feldman, *Dielectric relaxation in biological systems: Physical principles, methods, and applications*. Academic, 2015.

[17] K. Vinoth, T. Ganesh, P. Senthil Kumar, M. Maria Sylvester, D. Anand Karunakaran, A. Ramrao Deshmukh, and A. Kumbharkhane, "Molecular dynamics and dielectric relaxation by drs, calorimetric analysis and spectral inferences of amino acid complexes," *Chemical Physics Letters*, vol. 731, p. 136585, 2019.

[18] J. Průša and M. Cifra, "Dependence of amino-acid dielectric relaxation on solute-water interaction: Molecular dynamics study," *Journal of Molecular Liquids*, vol. 303, p. 112613, 2020.

[19] B. Naseem, I. Arif, and M. A. Jamal, "Kosmotropic and chaotropic behavior of hydrated ions in aqueous solutions in terms of expansibility and compressibility parameters," *Arabian Journal of Chemistry*, vol. 14, no. 11, p. 103405, 2021.

[20] Y. Marcus, "Effect of ions on the structure of water," *Pure and Applied Chemistry*, vol. 82, no. 10, pp. 1889–1899, 2010.

[21] V. Balos, B. Marekha, C. Malm, M. Wagner, Y. Nagata, M. Bonn, and J. Hunger, "Specific ion effects on an oligopeptide: Bidentate binding matters for the guanidinium cation," *Angewandte Chemie International Edition*, vol. 58, no. 1, pp. 332–337, 2019.

[22] D. J. Tobias and J. C. Hemminger, "Getting specific about specific ion effects," *Science*, vol. 319, no. 5867, pp. 1197–1198, 2008.

[23] J. D. Smith, R. J. Saykally, and P. L. Geissler, "The effects of dissolved halide anions on hydrogen bonding in liquid water," *Journal of the American Chemical Society*, vol. 129, no. 45, pp. 13847–13856, 2007.

[24] A. R. Leach, *Molecular modelling : principles and applications*. Harlow [u.a.]: Pearson, Prentice Hall, 2. ed. ed., 2001.

[25] J. W. Schultz, "Dielectric spectroscopy in analysis of polymers," *Encyclopedia of Analytical Chemistry: Applications, Theory and Instrumentation*, 2006.

[26] C. Schröder and O. Steinhauser, "Using fit functions in computational dielectric spectroscopy," *The Journal of Chemical Physics*, vol. 132, p. 244109, 06 2010.

[27] A. Szabadi, P. Honegger, F. Schöfbeck, M. Sappl, E. Heid, O. Steinhauser, and C. Schröder, "Collectivity in ionic liquids: a temperature dependent, polarizable molecular dynamics study," *Phys. Chem. Chem. Phys.*, vol. 24, pp. 15776–15790, 2022.

[28] F. Kremer and A. Schönhals, *Broadband Dielectric Spectroscopy*. Springer Berlin, Heidelberg, first ed., 2002.

[29] K. Asami, "Characterization of heterogeneous systems by dielectric spectroscopy," *Progress in Polymer Science*, vol. 27, no. 8, pp. 1617–1659, 2002.

[30] K. Grenier, D. Dubuc, T. Chen, F. Artis, T. Chretiennot, M. Poupot, and J.-J. Fournié, "Recent advances in microwave-based dielectric spectroscopy at the cellular level for cancer investigations," *IEEE Transactions on Microwave Theory and Techniques*, vol. 61, no. 5, pp. 2023–2030, 2013.

[31] H. M. Fahmy, A. M. Hamad, F. A.-z. Sayed, Y. S. Abdelaziz, E. S. Abu Serea, A. B. E.-D. Mustafa, M. A. Mohammed, and A. M. Saadeldin, "Dielectric spectroscopy signature for cancer diagnosis: A review," *Microwave and Optical Technology Letters*, vol. 62, no. 12, pp. 3739–3753, 2020.

[32] G. Floudas, "2.32 - dielectric spectroscopy," in *Polymer Science: A Comprehensive Reference* (K. Matyjaszewski and M. Möller, eds.), pp. 825–845, Amsterdam: Elsevier, 2012.

[33] M. Soltani and M. Omid, "Detection of poultry egg freshness by dielectric spectroscopy and machine learning techniques," *LWT - Food Science and Technology*, vol. 62, no. 2, pp. 1034–1042, 2015.

[34] M. Soltani Firouz, M. Rashvand, and M. Omid, "Rapid identification and quantification of sesame oils adulteration using low frequency dielectric spectroscopy combined with chemometrics," *LWT*, vol. 140, p. 110736, 2021.

[35] D. Malleo, J. T. Nevill, A. van Ooyen, U. Schnakenberg, L. P. Lee, and H. Morgan, "Note: Characterization of electrode materials for dielectric spectroscopy," *Review of Scientific Instruments*, vol. 81, p. 016104, 01 2010.

[36] C. Schröder, T. Rudas, G. Neumayr, W. Gansterer, and O. Steinhauser, "Impact of anisotropy on the structure and dynamics of ionic liquids: A computational study of 1-butyl-3-methyl-imidazolium trifluoroacetate," *The Journal of Chemical Physics*, vol. 127, p. 044505, 07 2007.

[37] G. R. Leader and J. F. Gormley, "The dielectric constant of n-methylamides," *Journal of the American Chemical Society*, vol. 73, no. 12, pp. 5731–5733, 1951.

[38] L. Martínez, R. Andrade, E. G. Birgin, and J. M. Martínez, "Packmol: A package for building initial configurations for molecular dynamics simulations," *Journal of Computational Chemistry*, vol. 30, no. 13, pp. 2157–2164, 2009.

[39] P. Eastman, J. Swails, J. D. Chodera, R. T. McGibbon, Y. Zhao, K. A. Beauchamp, L.-P. Wang, A. C. Simmonett, M. P. Harrigan, C. D. Stern, R. P. Wiewiora, B. R. Brooks, and V. S. Pande, "Openmm 7: Rapid development of high performance algorithms for molecular dynamics," *PLOS Computational Biology*, vol. 13, pp. 1–17, 07 2017.

[40] S. Jo, T. Kim, V. G. Iyer, and W. Im, "Charmm-gui: A web-based graphical user interface for charmm," *Journal of Computational Chemistry*, vol. 29, no. 11, pp. 1859–1865, 2008.

[41] B. R. Brooks et al., "Charmm: The biomolecular simulation program," *Journal of Computational Chemistry*, vol. 30, no. 10, pp. 1545–1614, 2009.

[42] A. Silva and W. Vranken, "Acpype-antechamber python parser interface," *BMC research notes*, vol. 5, p. 367, 07 2012.

[43] C. Fellinger, "Computational analysis of arginine in saline solution via dielectric spectroscopy," Master's thesis, University of Vienna, 2022.

[44] J. A. Maier et al., "ff14sb: Improving the accuracy of protein side chain and backbone parameters from ff99sb," *Journal of Chemical Theory and Computation*, vol. 11, no. 8, pp. 3696–3713, 2015.

[45] J. A. Maier, C. Martinez, K. Kasavajhala, L. Wickstrom, K. E. Hauser, and C. Simmerling, "ff14sb: Improving the accuracy of protein side chain and backbone parameters from ff99sb," *Journal of Chemical Theory and Computation*, vol. 11, no. 8, pp. 3696–3713, 2015.

[46] N. Michaud-Agrawal, E. J. Denning, T. B. Woolf, and O. Beckstein, "Mdanalysis: A toolkit for the analysis of molecular dynamics simulations," *Journal of Computational Chemistry*, vol. 32, no. 10, pp. 2319–2327, 2011.

[47] T. Hansson, C. Oostenbrink, and W. van Gunsteren, "Molecular dynamics simulations," *Current Opinion in Structural Biology*, vol. 12, no. 2, pp. 190–196, 2002.

[48] M. Gonzalez and J. Abascal, "The shear viscosity of rigid water models," *The Journal of chemical physics*, vol. 132, p. 096101, 03 2010.

[49] Y. Song and L. L. Dai, "The shear viscosities of common water models by non-equilibrium molecular dynamics simulations," *Molecular Simulation*, vol. 36, no. 7-8, pp. 560–567, 2010.

[50] G. Hefter and R. Buchner, "Dielectric relaxation spectroscopy: an old-but-new technique for the investigation of electrolyte solutions," *Pure and Applied Chemistry*, vol. 92, no. 10, pp. 1595–1609, 2020.

[51] D. Braun, S. Boresch, and O. Steinhauser, "Transport and dielectric properties of water and the influence of coarse-graining: Comparing BMW, SPC/E, and TIP3P models," *The Journal of Chemical Physics*, vol. 140, p. 064107, 02 2014.

[52] P. Höchtl, S. Boresch, W. Bitomsky, and O. Steinhauser, "Rationalization of the dielectric properties of common three-site water models in terms of their force field parameters," *The Journal of Chemical Physics*, vol. 109, pp. 4927–4937, 09 1998.

[53] C. Schröder, "Proteins in Ionic Liquids: Current Status of Experiments and Simulations," *Topics in Current Chemistry*, vol. 375, 02 2017.

[54] G. Camisasca, H. Pathak, K. T. Wikfeldt, and L. G. M. Pettersson, "Radial distribution functions of water: Models vs experiments," *The Journal of Chemical Physics*, vol. 151, p. 044502, 07 2019.

[55] C. Zhang and G. Galli, "Dipolar correlations in liquid water," *The Journal of Chemical Physics*, vol. 141, p. 084504, 08 2014.